Journal of Theoretical Biology 347 (2014) 17–32

Contents lists available at ScienceDirect

Journal of Theoretical Biology

journal homepage: www.elsevier.com/locate/yjtbi

Modelling the coupling between intracellular calcium release and the cell cycle during cortical brain development

Duncan S. Barrack [a,b,*], Rüdiger Thul [b], Markus R. Owen [b]

[a] Horizon Digital Economy Research Institute, University of Nottingham, Nottingham NG7 2TU, UK
[b] School of Mathematical Sciences and Centre for Mathematical Medicine and Biology, University of Nottingham, Nottingham, UK

HIGHLIGHTS

- We present a new model for ATP mediated coupling of calcium and cell cycle dynamics.
- Bifurcation analysis shows region of multistability of fixed points and limit cycles.
- Continuation and simulations reveal weak dependence of cell cycle period on calcium.
- Multistability allows cycling cells to recruit quiescent cells onto the cell cycle.
- Such recruitment could explain observed increases in cell proliferation rate.

ARTICLE INFO

Article history:
Received 5 April 2013
Received in revised form
28 November 2013
Accepted 3 January 2014
Available online 13 January 2014

Keywords:
Cell cycle
Calcium dynamics
Radial glial cells
Bifurcation analysis

ABSTRACT

Most neocortical neurons formed during embryonic brain development arise from radial glial cells which communicate, in part, via ATP mediated calcium signals. Although the intercellular signalling mechanisms that regulate radial glia proliferation are not well understood, it has recently been demonstrated that ATP dependent intracellular calcium release leads to an increase of nearly 100% in overall cellular proliferation. It has been hypothesised that cytoplasmic calcium accelerates entry into S phase of the cell cycle and/or acts to recruit otherwise quiescent cells onto the cell cycle. In this paper we study this cell cycle acceleration and recruitment by forming a differential equation model for ATP mediated calcium-cell cycle coupling via Cyclin D in a single radial glial cell.

Bifurcation analysis and numerical simulations suggest that the cell cycle period depends only weakly on cytoplasmic calcium. Therefore, the accelerative impact of calcium on the cell cycle can only account for a small fraction of the large increase in proliferation observed experimentally. Crucially however, our bifurcation analysis reveals that stable fixed point and stable limit cycle solutions can coexist, and that calcium dependent Cyclin D dynamics extend the oscillatory region to lower Cyclin D synthesis rates, thus rendering cells more susceptible to cycling. This supports the hypothesis that cycling glial cells recruit quiescent cells (in G_0 phase) onto the cell cycle, via a calcium signalling mechanism, and that this may be the primary means by which calcium augments proliferation rates at the population scale. Numerical simulations of two coupled cells demonstrate that such a scenario is indeed feasible.

1. Introduction

Radial glial cells are transient cells, only present in the mammalian brain for a brief period during embryonic development. During this time they give rise to neurons (Noctor et al., 2001) and in doing so play a major role in the development of the neocortex. A recent study reveals that calcium waves which propagate through the ventricular zone of the embryonic brain enhance radial glial cell proliferation (Weissman et al., 2004). In this study Weissman et al. hypothesised that ATP mediated calcium release in radial glia may accelerate G_1 progression of the cell cycle and/or act to recruit cells otherwise destined to enter the G_0 resting phase on to the cell cycle.

The radial glial cell cycle, like that of any eukaryotic cell, can be broken down into several phases (Murray and Hunt, 1993). G_1 phase is the period of greatest growth and is the longest phase, approximately half the total cell cycle period in most cell types. It is when a cell pauses during G_1 that it enters the quiescent state, G_0. Otherwise, G_1 is followed by S phase, during which DNA replication occurs, and then G_2, during which the cell prepares for mitosis (M phase). Shortly after M phase, the parent cell separates into two daughter cells, completing the cell cycle.

The cell cycle is controlled by a large number of biochemical regulators including Cyclins and Cyclin dependent kinases (Cdks). Cdks phosphorylate target proteins when paired up with respective

* Corresponding author at: Horizon Digital Economy Research Institute, University of Nottingham, Nottingham NG7 2TU, UK. Tel.: +44 115 8232554.
E-mail address: duncan.barrack@nottingham.ac.uk (D.S. Barrack).

0022-5193/$ - see front matter © 2014 Elsevier Ltd. All rights reserved.
http://dx.doi.org/10.1016/j.jtbi.2014.01.004

Cyclin partners. Phosphorylated proteins facilitate numerous cell cycle events including DNA replication and chromosome condensation. There is usually a constant amount of Cdks during the cell cycle and consequently Cdk activity is highly dependent upon the availability of their Cyclin partners which are produced and degraded as needed (Nigg, 1995).

Numerous studies using different cell types suggest that the activity of Cyclin D, which plays a crucial role in driving the cell through G_1 (Baldin et al., 1993) and towards S phase, increases in the presence of active calcium/calmodulin dependent kinases (CaMK) (Kahl and Means, 2003, 2004; Morris et al., 1998; Tombes et al., 1995; Rasmussen and Rasmussen, 1995) and this is thought to be a major pathway by which intracellular calcium release can affect the cell cycle. Calcium, via CaMK, can also aid M phase entry and progression by increasing the activity of the cell cycle phosphatase Cdc25 at the G2/M phase transition (Patel et al., 1999; Swanson et al., 1997; Kahl and Means, 2003) or by indirectly affecting Cdk1 activity during M phase (Suprynowicz et al., 1994).

In radial glia, calcium release is initiated by the binding of extracellular adenosine triphosphate (ATP) to $P2Y_1$ receptors, which leads, via a G-protein cascade, to inositol 1,4,5-trisphosphate (IP_3) mediated calcium release from the endoplasmic reticulum (ER) into the cytosol (Weissman et al., 2004). ATP is released from cells through hemichannels (Li et al., 1996) which allow for molecular transport between the cytosol and the extracellular space. Hemichannels, formed via the separation of gap junctions between adjacent cells, assemble sometime between G_1 and early S phase (Bittman and LoTurco, 1999; Goto et al., 2002; Weissman et al., 2004). In Fig. 1, we summarise how ATP leads to the release of calcium in radial glia and the effect of calcium on G_0 and G_1 phases of the cell cycle.

Although Weissman et al. (2004) did not measure directly the increase in cell proliferation rate in the presence of ATP mediated calcium signalling, their results allow us to obtain an estimate for the increase. In their experiments, Bromodeoxyuridine (BrdU) was added to cultures of radial glia which had been exposed to suramin over an observation period of one hour. BrdU, which is incorporated into DNA by cycling cells during S phase, serves as a marker of proliferation. Suramin, an ATP receptor antagonist, acted to abolish ATP mediated calcium release in radial glial. Weissman et al. observed that, during the hourly period, the proportion of cells labelled with BrdU (and hence having entered S Phase) was 54.7% that of the case where the ATP receptors of cells were allowed to function as normal. Therefore 45.3% of the cells which entered S phase during the hourly observation period for the case with normally functioning ATP receptor activity would not have done so if it were not for ATP mediated calcium. Under the assumption that the number of cells which have entered S phase over a short period of time can be used as a proxy for the radial glial proliferation rate, this corresponds to an increase of 82.8% (45.3/54.7) in the rate of proliferation brought about by ATP mediated calcium. An approximate doubling in cellular proliferation rate of radial glia is consistent with other studies conducted on neural progenitor cells. In particular, Mishra et al. (2006) demonstrated that, over a 7 day period, the total cell count of wild type murine sub-ventricular zone progenitor cells in which ATP mediated calcium release was permitted was approximately double that of cells in which $P2Y_1$ ATP receptors were knocked out.

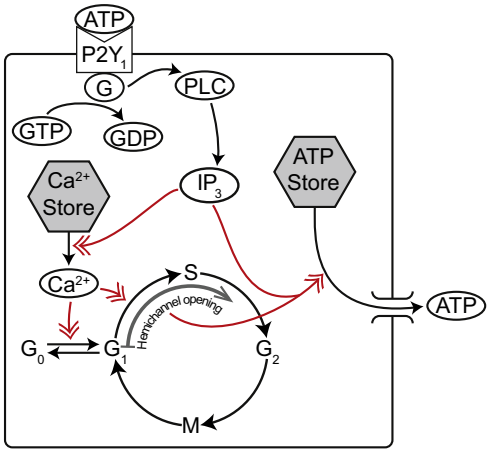

Fig. 1. Schematic illustration of how ATP causes calcium to be released and how calcium affects G_0 and G_1 phases of the cell cycle in radial glia. Arrows indicate regulatory interactions, with red arrows signifying key interactions. ATP bound $P2Y_1$ receptors activate a G-protein molecular switch, whereby G-proteins exchange guanosine diphosphate (GDP) for guanosine triphosphate (GTP). This in turn leads, via the phospholipase-C (PLC) pathway, to the production of IP_3. IP_3 allows for the release of ATP and facilities the liberation of calcium from internal stores. Free calcium has the effect of inducing a cell to enter S phase from G_1 and/or recruiting a cell in G_0 onto the cell cycle. During G_1 or S phase, hemichannels open, allowing for the release of ATP into the extracellular space. (For interpretation of the references to colour in this figure caption, the reader is referred to the web version of this paper.)

In this paper, to investigate how calcium signals lead to an increase in overall cellular proliferation, we couple an existing cell cycle model to a modified model for ATP mediated calcium release. We consider two forms of coupling in order to capture different ATP release patterns. Furthermore, because calcium spikes are rapid compared to the period of cell cycle oscillations, we incorporate time averaged calcium dynamics into the model (See Appendix A for details). Although several deterministic models of the cell cycle exist (see Csikász-Nagy, 2009 for an excellent review) and more recently a number of models for ATP mediated calcium signalling in astrocytes have been developed (Bennett et al., 2005; Stamatakis and Mantzaris, 2006; Wang et al., 2007), to our knowledge, ours is the first model which couples cell cycle dynamics to mechanistic calcium release (but see Dupont, 1998 for a model that couples prescribed calcium spikes to meiotic cell division). Analysis of our model suggests that the modulations in cell cycle period brought about by calcium can only account for a small proportion of the increase in cellular proliferation observed experimentally. However, bifurcation results and simulation results of two cell systems indicate that the possibility for cycling cells to recruit quiescent cells onto the cell cycle via ATP mediated calcium release is viable and this process could be the dominant mechanism by which intracellular calcium impacts proliferation rates within a population of cells.

The paper is structured as follows. In Section 2, we present the single cell model and in Section 3 we study the dynamics of it via bifurcation analysis and numerical simulations. We conclude with a discussion in Section 4.

2. Model formulation

We couple the model of Obeyesekere et al. (1999) for the mammalian cell cycle to an adapted version of the model of Bennett et al. (2005) for ATP mediated calcium release, to form a model for coupled calcium-cell cycle dynamics in a single non-differentiating radial glial cell. The cell cycle model of Obeyesekere et al. is given by

$$\frac{dD}{dt} = a_d \cdot GF - d_D ED, \tag{1}$$

$$\frac{dE}{dt} = a_E(1 + a_f(E2F_T - R_s)) - d_E XE, \tag{2}$$

$$\frac{dR}{dt} = \frac{p_X(R_T - R_s - R)X}{q_X + (R_T - R_s - R) + X} - p_s(E2F_T - R_s)R, \tag{3}$$

$$\frac{dR_s}{dt} = p_s(E2F_T - R_s)R - \frac{p_D R_s D}{q_D + R_s + D} - \frac{p_E R_s E}{q_E + R_s + E}, \tag{4}$$

$$\frac{dX}{dt} = a_X E + \beta(E2F_T - R_s) + gX^2 E - d_X X. \tag{5}$$

In this system of ordinary differential equations (ODEs), D and E are, respectively, the average concentrations of active Cyclin D/Cdk4 and Cyclin E/Cdk2 dimers. Cdks are assumed to be available in abundance and as soon as Cyclins are produced they bind to their respective Cdk partners (henceforth, we use the phrases 'active Cyclin' and 'active Cyclin/Cdk dimers' interchangeably). R is retinoblastoma tumour suppressor protein (RB) in its unphosphorylated form and R_s is RB bound to the E2F transcription factor. Like the Cdks, the total concentrations of RB (R_T) and E2F ($E2F_T$) are assumed to be constant throughout the cell cycle. X is the 'cell progression indicator' (CPI) which indirectly represents the kinases, phosphatases and proteases responsible for driving the cell through the S, G_2 and M phases of the cell cycle. In lumping together various cellular processes in this manner, the dimensionality of the model can be reduced without loosing too much accuracy.

In Eq. (1), growth factor activity (GF) (Aktas et al., 1997; Sherr, 1994) stimulates Cyclin D production with rate parameter a_d and, based on evidence that Cyclin/Cdk complexes can promote Cyclin degradation in G_1 (Lanker et al., 1996), it is assumed that Cyclin E indirectly promotes Cyclin D degradation with rate constant d_D. This latter assumption is consistent with experiments showing that Cyclin E/Cdk2 can phosphorylate the Cdk inhibitor $p27^{kip1}$, marking it for degradation (Sheaff et al., 1997). As $p27^{kip1}$ is an essential activator of Cyclin D dependent kinases (Cheng et al., 1999), Cyclin E/Cdk2 can indirectly inhibit Cyclin D/Cdk4 activity via this pathway. In Eq. (2), free E2F ($E2F_T - R_s$), liberated from RB/E2F complexes, acts to promote Cyclin E production with rate parameters a_E and a_f and the CPI degrades Cyclin E with rate constant d_E. The terms in Eqs. (3) and (4) represent dephosphorylation of RB and binding of unphosphorylated RB to the E2F transcription factor. In Eq. (3) the CPI dephosphorylates RB according to Michaelis–Menten type kinetics with maximum rate parameter p_X and Michaelis constant q_X. In Eq. (4) both active Cyclin D and active Cyclin E phosphorylate RB with maximum rate parameters p_D and p_E respectively and Michaelis constants q_D and p_E respectively. Although Cyclin D and Cyclin E phosphorylate free RB which is not in a complex with E2F as well these pathways are not included in the model and their omission has no effect on the results of the cell cycle model (Obeyesekere et al., 1999). Additionally, in Eq. (4) RB/E2F (R_s) forms via binding of free E2F to RB with rate constant p_s. In Eq. (5), the CPI, which decays at rate d_X, is produced in response to Cyclin E (with rate parameter a_X), free E2F (with rate parameter β) and, in an autocatalytic manner, by itself and active Cyclin E (with rate parameter g).

We chose the model of Obeyesekere et al. primarily because it includes Cyclin D (a key target of CaMK signalling). In addition this model is low dimensional which renders it an ideal starting point for coupling cell cycle and intracellular calcium dynamics for the first time. To the best of our knowledge the only other models which incorporate Cyclin D are due to Novak and Tyson (2004), Swat et al. (2004), Chauhan et al. (2008, 2011), Gérard and Goldbeter (2009) and Pfeuty (2012). However these models are significantly more complex. For example the model by Novak and Tyson has more than four times as many variables and three times as many parameters as the model of Obeyesekere et al. and the model by Gérard and Goldbeter has nearly eight times as many variables and more than nine times as many parameters. The model of Chauhan et al. includes regulatory pathways specific to mammalian liver damage and because of this it is not a suitable model for the radial glial cell cycle.

As there is evidence that calcium, via the activation of CaMK, increases Cyclin D activity in several cell types (Kahl and Means, 2003, 2004; Morris et al., 1998; Tombes et al., 1995; Rasmussen and Rasmussen, 1995) we make Cyclin D synthesis an increasing function of calcium in the cell. In addition calcium interacts with other cell cycle proteins such as Cdc25 (Patel et al., 1999; Kahl and Means, 2003) and Cdk1 (Suprynowicz et al., 1994). However we do not consider the impact of calcium on these proteins here as their effect is either felt at the entry to, or during M phase and the focus of this work is on the effect of calcium on the G_0/G_1 and G_1/S transitions in radial glia. For these transitions, Cyclin D which drives G_1 progression is the key cell cycle protein. We use the following coupling for calcium and the Cyclin D synthesis rate term a_d from Eq. (1):

$$a_d([Ca^{2+}]) = a_d' + \gamma([Ca^{2+}] - [Ca^{2+}]_b). \tag{6}$$

In this expression γ is the strength of the coupling to the intracellular calcium concentration and $[Ca^{2+}]_b$ is a constant representing the steady state cytosolic concentration of calcium for the calcium release model (Eq. (15)).

On the grounds that radial glial cells and astrocytes share many molecular and cellular characteristics (Gotz and Barde, 2005), such as ATP dependent intracellular calcium release (Fam et al., 2003; Hung and Colicos, 2008), we model ATP mediated calcium release in radial glia by adapting the model of Bennett et al. (2005) for ATP mediated calcium waves in astrocytes. In the model of Bennett et al. extracellular ATP receptor and G-protein activity are described by

$$\rho = \frac{[ATP_E]}{K_R + [ATP_E]} \quad \text{and} \quad G^* = \frac{\rho + \nu}{K_G + \rho + \nu}. \tag{7}$$

In Eq. (7), ρ is the fraction of bound $P2Y_1$ receptors, $[ATP_E]$ the concentration of extracellular ATP and K_R the dissociation constant for ATP receptor binding. G^* is the proportion of active G-protein, ν is the background G-protein activation in the absence of ATP and K_G is the dissociation constant. IP_3 and ATP dynamics are modelled by

$$\frac{d[IP_3]}{dt} = r_h^* G^* - k_{deg}[IP_3], \tag{8}$$

$$\frac{d[ATP_I]}{dt} = ATP_{prod} - ATP_{rel}, \tag{9}$$

$$\frac{d[ATP_E]}{dt} = ATP_{rel} - ATP_{deg}. \tag{10}$$

In this set of ODEs, r_h^* and k_{deg} are, respectively, the production and degradation rates of IP_3 ($[IP_3]$). ATP_{prod}, an addition to the original model of Bennett et al. in which intracellular ATP production is not considered, is the production of intracellular ATP ($[ATP_I]$). ATP_{rel} is the ATP release into extracellular space and ATP_{deg} the degradation of extracellular ATP. The expressions for these three terms are given by

$$ATP_{prod} = \alpha([ATP_I]_{max} - [ATP_I]), \tag{11}$$

$$ATP_{deg} = V_{deg}\frac{[ATP_E]}{K_{deg} + [ATP_E]}, \tag{12}$$

$$ATP_{rel} = \left(\frac{[IP_3] - [IP_3]_{min}}{K_{rel} + [IP_3]}\right) V_{ATP}([ATP_I] - [ATP_E])T(i_1 - i_2)T([IP_3] - [IP_3]_{min}). \tag{13}$$

In Eq. (11), α is the rate constant for ATP production and $[ATP_I]_{max}$ the maximum intracellular concentration of ATP. Eq. (12) describes extracellular ATP degradation which is modelled according to Michaelis–Menten kinetics with parameters V_{deg} and K_{deg}. Following experimental evidence (Bennett et al., 2005) the

$([IP_3]-[IP_3]_{min})/(K_{rel}+[IP_3])$ term from Eq. (13) ensures that ATP release is dependent upon IP_3 with a sensitivity concentration of K_{rel}. $([ATP_I]-[ATP_E])$ models passive transport through open hemichannels and V_{ATP} is the rate constant for ATP release when hemichannels are open. In keeping with the model of Bennett et al., the IP_3 concentration must exceed a threshold value $[IP_3]_{min}$ before ATP is released. For our model, we introduce the function T into Eq. (13) to model both switch-like IP_3 dependent ATP release and switch-like hemichannel opening, with T defined by

$$T(x)=\frac{1}{2}\left(\tanh\left(\frac{x}{\varepsilon}\right)+1\right), \tag{14}$$

where ε is a stiffness parameter. In Eq. (13), i_1 and i_2 are either the concentration, or the parameter representing the critical concentration, of one of the cell cycle variables from (1)–(5). If i_1 (*resp.* i_2) is a variable, then hemichannel opening and subsequent ATP release occurs when that variable exceeds (falls below) a threshold parameter i_2 (i_1). As different proteins peak and dip at different times during the cell cycle, the choice of i_1 and i_2 allows us to model ATP release at specific times.

Evidence from the literature suggests that hemichannel opening and consequent ATP release occurs in G_1 or S phase of the cell cycle. With this in mind, we consider two model variants. In the first variant, ATP release occurs towards mid G_1 phase, and in the second, release occurs later, towards the G_1/S phase transition. As Cyclin D peaks during G_1 phase before dropping off in S phase in the mammalian cell cycle (Chen et al., 2005; Stacey, 2003; Yang et al., 2006), we model ATP release during mid G_1 phase by setting $i_1=D$ and $i_2=D_c$ in Eq. (13), where D_c is the critical concentration of Cyclin D which must be exceeded for ATP to be released. We refer to this model as the 'Cyclin D dependent ATP release model variant'. Late G_1 phase is associated with low concentrations of bound RB/E2F (Greenblatt, 2005; Sinal and Woods, 2005; Veylder et al., 2003), so we model the release of ATP at the G_1/S transition by choosing $i_1=R_{sc}$ and $i_2=R_s$, where R_{sc} is the critical R_s concentration below which ATP is released. We refer to this as the 'R_s dependent ATP release model variant'.

Bennett et al. use a model for calcium release originally developed by Li and Rinzel (1994) where IP_3 stimulates intracellular calcium release. As extracellular calcium does not contribute to calcium elevations in radial glia (Weissman et al., 2004), this model is sufficient to describe calcium dynamics in our study. In the calcium release model, for certain parameter values, release is oscillatory with period of oscillation of the order of seconds. Such a time scale is consistent with the oscillatory period of calcium release in radial glia (Weissman et al., 2004). However, in this paper we are interested in the effect calcium has on the cell cycle which has a period of oscillation of the order of tens of hours. Because of this, and for the reason that no process is slaved to the fast calcium oscillations, as detailed in Appendix A, we replace oscillatory calcium release with a functional fit to give the following expression for IP_3 dependent calcium release from the ER:

$$[Ca^{2+}]=[Ca^{2+}]_b+\frac{p_1[IP_3]^m}{p_2^m+[IP_3]^m}+\frac{p_3[IP_3]^n}{p_4^n+[IP_3]^n}. \tag{15}$$

This simplification gives a considerable saving in computational simulation time, but minimal loss of accuracy, as illustrated in Appendix A.

To summarise the dynamics outlined above, the $T(i_1-i_2)$ term in Eq. (13) regulates hemichannel opening and ATP release. The point during the cell cycle at which this occurs is determined by the cell cycle variables, whose dynamics are governed by Eqs. (1)–(5). Extracellular ATP leads to an increase in the number of bound receptors (ρ in Eq. (7)), which in turn leads to an increase in G-protein activity (G^* in Eq. (7)). This results, via IP_3 production (Eq. (8)), in the release of calcium from internal stores (Eq. (15)). Cytosolic calcium then acts to increase Cyclin D activity (Eq. (6)). ATP release is triggered by one of the cell cycle variables either exceeding or falling below a critical value (Eq. (13)) and the process begins anew. For readability the model equations are reproduced in Appendix B. The model is also publicly available for download in SMBL format from the BioModels database (BioModels ID: MODEL1401200000 and MODEL1401200001). A wiring diagram of all model variables is included in Appendix C and in Appendix D we provide the parameter values used in our model with details of their derivation.

3. Model analysis

In this section, we subject both model variants to bifurcation analysis and numerical simulations in order to uncover their dynamics. We begin by conducting bifurcation analysis using the intrinsic Cyclin D synthesis rate a_d' as the control parameter. a_d' plays a crucial role in our model as it affects the frequency of oscillation of the cell cycle and can control whether the model oscillates at all. Fig. 2 shows bifurcation diagrams for the Cyclin D dependent ATP release and R_s dependent ATP release model variants for coupled ATP mediated calcium-cell cycle dynamics in a single radial glial cell (black symbols). We refer to this version as the 'ATP coupled' case. For purposes of comparison, an uncoupled cell cycle model without ATP mediated calcium-cell cycle coupling (achieved by setting the value for extracellular ATP ($[ATP_E]$) to 0) is also included (red symbols). We refer to this version as the 'ATP blocked' case and regard it as equivalent to the case in the experiment conducted by Weissman et al. (2004) where ATP receptor activity of radial glia was suppressed through the exposure of cells to suramin. We also note that the ATP blocked case is equivalent to the original cell cycle model of Obeyesekere et al. (1999). By comparing the cell cycle period of the ATP blocked case to the period of the model for the ATP coupled case, we will be able to determine the effect calcium has on the cell cycle period and, in turn, on the cellular proliferation rate of radial glia. For the ATP blocked case a supercritical Hopf bifurcation (HB) at $a_d'\approx 0.410$ leads to the creation of stable small amplitude oscillations. These are connected to a branch of stable large amplitude oscillations, with higher Cyclin D concentrations, via two saddle node bifurcations (FP1 at $a_d'\approx 0.424$ and FP2 at $a_d'\approx 0.395$). For the Cyclin D dependent ATP release variant of the ATP coupled case (Fig. 2(a and c), black symbols) additional pairs of saddle node bifurcations ($FP3^D$ at $a_d'\approx 0.396$ and $FP4^D$ at $a_d'\approx 0.385$) are created on the stable large amplitude solution branch. For R_s dependent ATP release (Fig. 2(b and d)), the saddle node bifurcation point from which large amplitude oscillations emerge occurs at a lower value for a_d' ($FP2^{Rs}$ at $a_d'\approx 0.345$) than is the case for the ATP blocked case. The pattern of behaviour for the Cyclin D dependent ATP release model variant, where additional pairs of saddle node bifurcations are present ($FP3^D$ and $FP4^D$), can also be seen for the R_s dependent variant. Which form is seen depends on whether ATP release begins on the unstable branch of oscillatory solutions between FP1 and FP2 or branch of stable solutions beyond FP2. Only when a cell is on the branch of large amplitude limit cycle solutions can it be regarded as cycling (Obeyesekere et al., 1999).

As can be seen in Fig. 2(c and d), ATP mediated calcium-cell cycle coupling (black symbols) brings about a decrease in cell cycle period compared to the ATP blocked case (red symbols). This reduction is modest however. For the baseline parameter values where $a_d'=0.41$, the reduction is 1.81 h (6.22% of the cell cycle period of the ATP blocked case) for the Cyclin D dependent model variant and 2.25 h (7.73%) for the R_s dependent model variant. These figures would correspond to an increase in the rate of

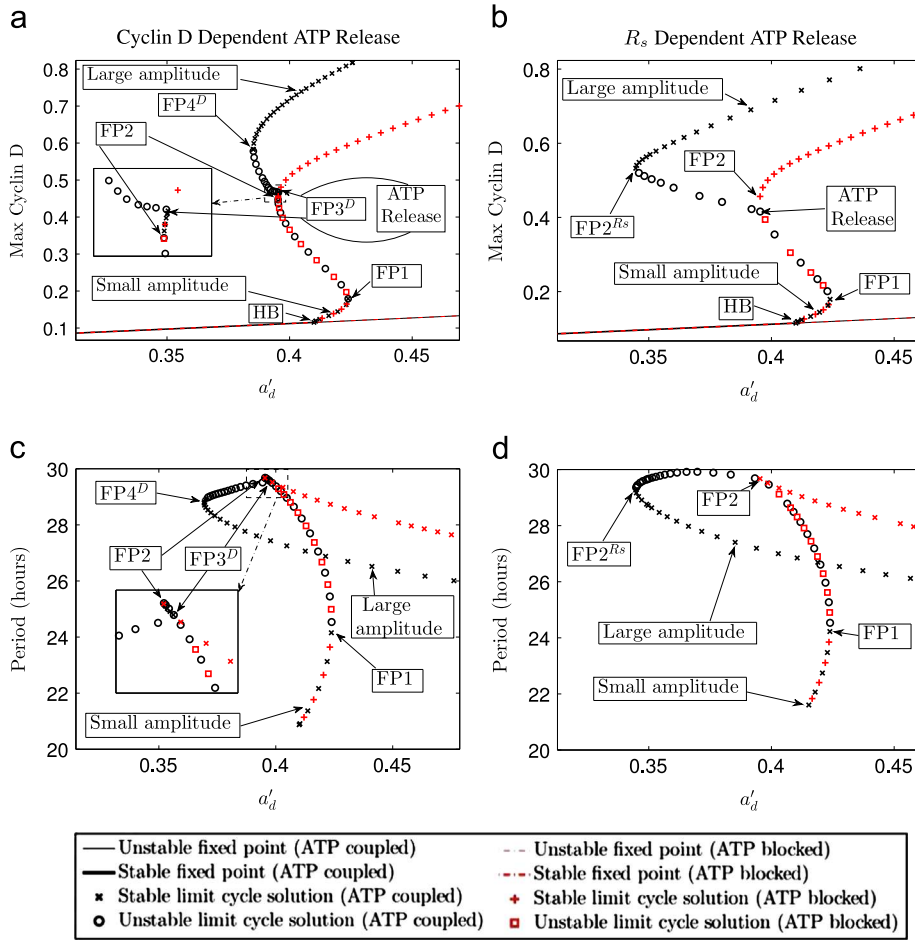

Fig. 2. Bifurcation diagrams of system (1)–(15) for ATP mediated calcium-cell cycle coupling in single radial glia showing maximum Cyclin D concentration and period of oscillation of limit cycle solutions as a function of the intrinsic Cyclin D synthesis rate a'_d. (a, c) correspond to the Cyclin D dependent ATP release model variant ($(i_1, i_2) = (D, D_c)$) and (b, d) to the R_s dependent ATP release model variant ($(i_1, i_2) = (R_{sc}, R_s)$). Superimposed on all plots are the results for the ATP blocked case with no ATP mediated calcium-cell cycle coupling (achieved by setting $[ATP_E] = 0$). FP1, FP2, $FP3^D$, $FP4^D$ and $FP2^{Rs}$ correspond to fold or saddle node bifurcation points, while HB corresponds to a Hopf bifurcation point. Points at which ATP is released in both variants are also indicated. Note, in (a) release, which occurs on the branch of unstable limit cycle solutions, is coincident with the bifurcation point $FP3^D$. The insets in (a, c) show details around FP2 and $FP3^D$. Parameter values as in Tables D1–D3 except for a'_d which is as shown. (For interpretation of the references to colour in the text, the reader is referred to the web version of this paper.)

proliferation brought about by ATP mediated calcium release of only 6.63% (i.e. 1.81/27.29) and 8.38% (2.25/26.85) respectively. In order to investigate more deeply the impact of calcium on cell cycle period we investigate how the period of oscillation of the large amplitude limit cycle solutions in Fig. 2 depends upon the calcium coupling strength γ and the critical concentrations, D_c and R_{sc}, at which ATP is released in both model variants. Bifurcation results are shown in Fig. 3 and, for all cases, the cell cycle period either has a local minimum (Fig. 3(a) at $\gamma \approx 4.25\ h^{-1}\ \mu M^{-1}$) or reaches an asymptotic value (Fig. 3(b–d)). For the parameter ranges illustrated in Fig. 3 the minimum cell cycle period is approximately 22.6 (a), 23.0 (b), 25.2 (c) and 25.2 (d) h. This represents a decrease in cell cycle period compared to the ATP blocked case of 6.5 ($\approx 22.2\%$), 6.1 ($\approx 21.1\%$), 3.9 ($\approx 13.4\%$), 3.9 ($\approx 13.4\%$) h respectively. However, for all these cases, such extreme parameter values lead to the saturation of the extracellular space with ATP for the entire, or almost the entire, period of the cell cycle. This is physically unrealistic as a constantly high ATP concentration is inconsistent with evidence from studies conducted on astrocytes in which it was demonstrated that the concentration of extracellular ATP rises and falls during the cell cycle according to a circadian rhythm (Womac et al., 2009; Marpegan et al., 2011).

In order to obtain an increase in the proliferation rate of 82.8% with ATP coupling, a reduction in cell cycle period of 45.3% compared to the ATP blocked case would be required. Therefore, when compared to the experimental work of Weissman et al. (from which the 82.8% figure was obtained) it becomes apparent that, for the results of Fig. 3, the decrease in period of cell cycle oscillations brought about by calcium can only, by itself, account for a small proportion of the experimentally observed large increase in overall cellular proliferation. However, the bifurcation results in Fig. 2(a and b) are consistent with the hypothesis that cycling cells may induce quiescent cells onto the cell cycle and this could be the primary means by which calcium signalling augments cellular proliferation. In particular, from Fig. 2(a and b), it can be seen that fixed point solutions (which correspond to the quiescent G_0 state (Obeyesekere et al., 1999)) and high amplitude limit cycle solutions (which correspond to the cycling state) coexist. ATP release from a cycling cell could induce calcium release in a dormant cell in G_0. Provided the calcium signal is of sufficient strength it could lift the quiescent cell onto the branch of limit cycle solutions. This could, in turn, lead to a large increase in cellular proliferation. We discuss this possibility further later in this section.

Next, to illustrate the large amplitude limit cycle solutions detected by the bifurcation analysis, we present the results of numerical simulations in Fig. 4. Oscillations in the model variables are clearly identifiable. ATP release duration is approximately 7.6 h in the Cyclin D dependent variant and approximately 13.7 h for the

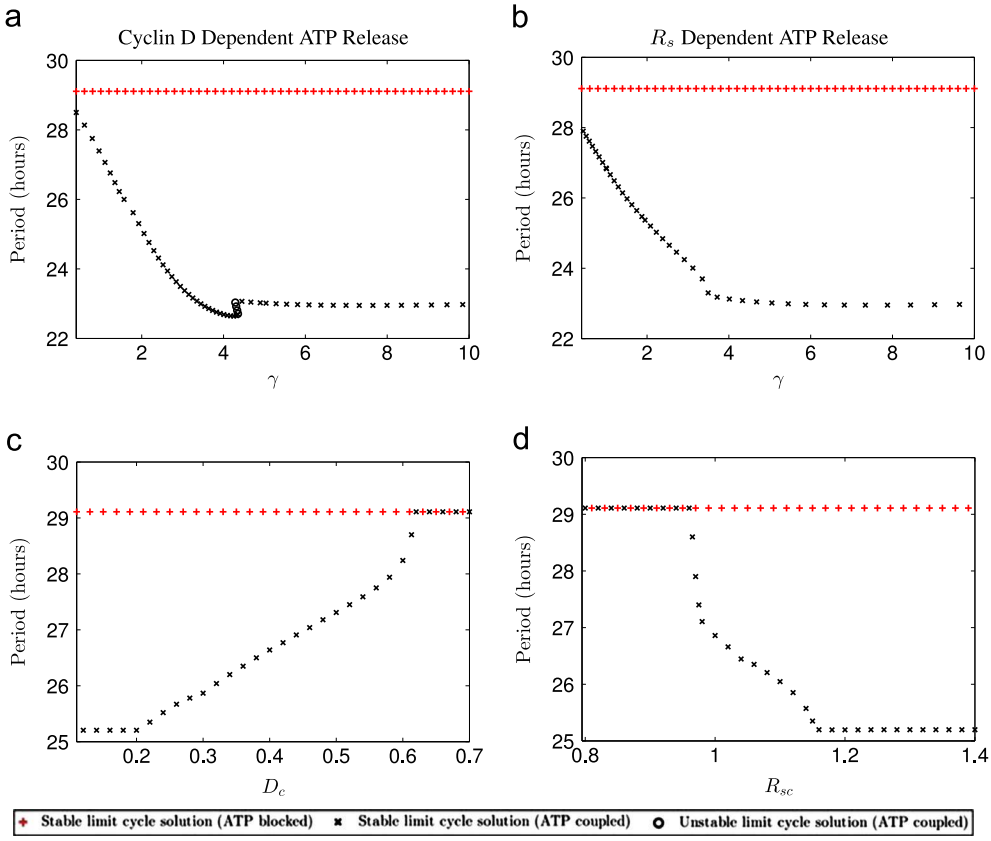

Fig. 3. Plots of the period of oscillation of the large amplitude stable limit cycle solutions shown in Fig. 2 as a function of the calcium coupling strength γ (a, b), and of the thresholds D_c and R_{sc} (c,d). (a, c) correspond to the Cyclin D dependent ATP release model variant ($(i_1, i_2) = (D, D_c)$) and (b, d) to the R_s dependent ATP release model variant ($(i_1, i_2) = (R_{sc}, R_s)$). Parameter values as in Tables D1–D3 except for (a, b): γ as shown and (c, d): D_c and R_{sc} as shown.

R_s dependent model variant. Although the literature is bereft of studies on the duration of ATP release in radial glia, studies of astrocytes suggest that ATP release can last from approximately 6 to 14 h (Womac et al., 2009; Marpegan et al., 2011), which is consistent with the aforementioned results for our model. The results in Fig. 4 also serve to illustrate that the timing and duration of ATP mediated calcium release differ between both variants. Although it is possible to vary parameter values so that the duration of ATP and calcium release is identical in both model variants, this will not yield identical cell cycle periods. Because the impact of calcium on the cell cycle dynamics is nonlinear, as well as duration, the timing of calcium release influences the dynamics. To illustrate the nonlinear effect of calcium, in Fig. 5 is shown an example where different underlying calcium dynamics give the same global response in the model. In particular, the duration of ATP mediated calcium release differs between both variants (9.9 h and 13.7 h for the Cyclin D dependent model and R_s dependent model variants respectively), but its affect on cell cycle period (which is 26.9 h in both cases) is identical.

To determine whether our observations that the cell cycle period shows a weak dependence on intracellular calcium are robust we carry out numerical simulations to investigate whether the oscillatory period shows a greater sensitivity to calcium when we change all parameter values which control various factors in our model such as IP_3 and ATP production (r_h^* and α respectively) and degradation (k_{deg} and K_{deg}, V_{deg} respectively). For each simulation we first generate a vector $\mathbf{P_j} = (P_1, \ldots, \lambda_j P_j, \ldots, P_{42})$, where the P_i, $i = 1, \ldots, 42$, refer to the baseline parameter values as indexed in Tables D1–D3. We then form another vector $\mathbf{P_{j,k}} = (P_1, \ldots, \lambda_j P_j, \ldots, \lambda_k P_k, \ldots, P_{42})$ where $k \neq j$. In both these vectors all entries correspond to the baseline values given in Tables D1–D3 except for a λ_j fold change of P_j in $\mathbf{P_j}$ and $\mathbf{P_{j,k}}$ as well as a λ_k fold change of P_k in $\mathbf{P_{j,k}}$. We then compute the maximal change in cell cycle period brought about by ATP mediated calcium release compared to the ATP blocked case, for a fixed value of λ_j, by varying λ_k over a large range, i.e.

$$L_k(\lambda_j) = \max_{\lambda_k}\left(\frac{L_0(\mathbf{P_j}) - L(\mathbf{P_{j,k}})}{L_0(\mathbf{P_j})}\right).$$

Here, $L_0(\mathbf{P_j})$ corresponds to the cell cycle period computed for the parameter regime $\mathbf{P_j}$ for the ATP blocked case. Similarly, $L(\mathbf{P_{j,k}})$ denotes the cell cycle period for the ATP coupled case for the parameter set $\mathbf{P_{j,k}}$.

Before presenting the results where all model parameters are varied from their baseline values we first illustrate the above procedure by choosing $P_j = K_{deg}$ and $P_k = \gamma$. Fig. 6 shows the proportional reduction in cell cycle period $(L_0(\mathbf{P_j}) - L(\mathbf{P_{j,k}}))/L_0(\mathbf{P_j})$ as a function of λ_j and λ_k. Our goal is to obtain the maximum reduction $L_k(\lambda_j)$ over all values of λ_k which is indicated by the green line in the figure.

The results where each parameter is varied, in turn, from its baseline value are shown in Fig. 7 where our choice of P_k mirrors our choice of the control parameters for the bifurcation analysis (see Fig. 3). For $P_k = \gamma$ (a,b) the results are very similar for both the model variants. In both cases the proportional reduction in period is relatively modest with a mean reduction over all parameter sets $\mathbf{P_j}$ for which limit cycle solutions exist of 0.158 (a) and 0.156 (b). For the instances where P_k is chosen to be the threshold parameters D_c (c) and R_{sc} (d), the results for both model variants are again very similar. Here, the mean proportional reduction in period is again relatively low (0.110 in (c) and 0.108 in (d)). These values are slightly lower than that was the case for the results in (a,b) reflecting the fact that the thresholds do not have as great an impact on cell cycle period as the calcium coupling strength γ.

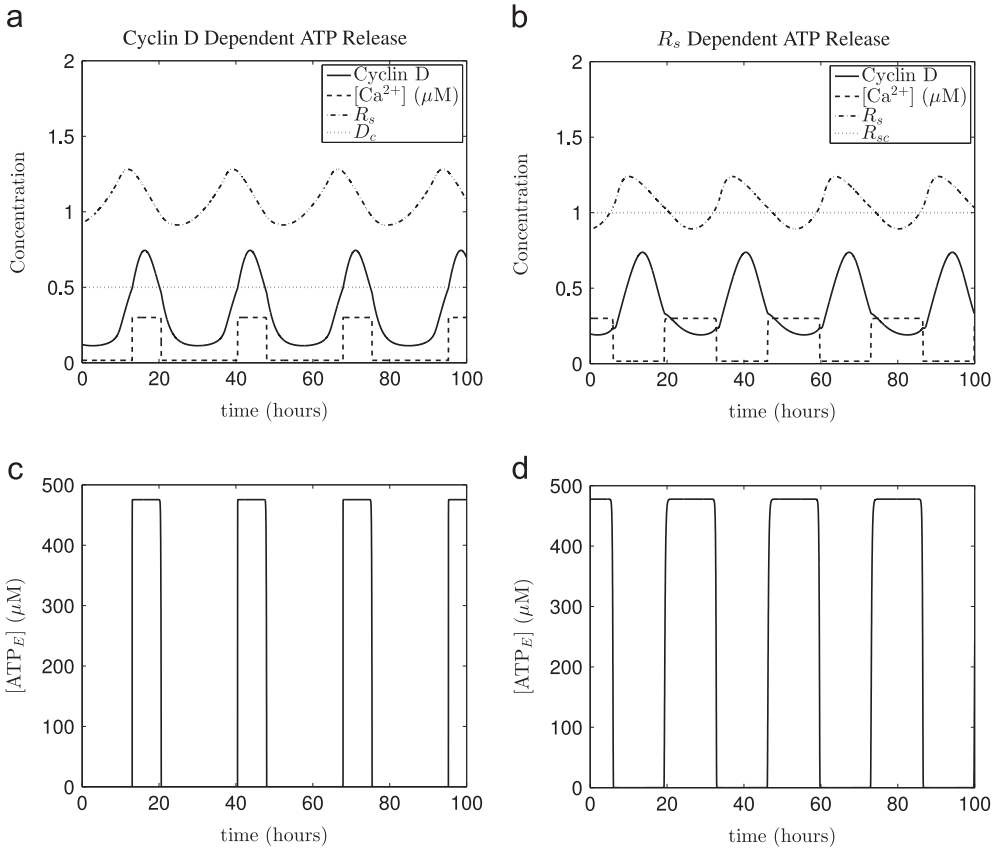

Fig. 4. Simulations of system (1)–(15) for calcium mediated cell cycle coupling in a single radial glial cell. (a, c) show ATP mediated calcium release occurring as Cyclin D is around its maximum (mid G_1 phase) in the Cyclin D dependent ATP release model ($(i_1, i_2) = (D, D_c)$). (b, d) show release occurring as R_s is close to its minimum (late G_1 phase) in the R_s dependent ATP release model ($(i_1, i_2) = (R_{sc}, R_s)$). Horizontal dotted lines show thresholds for ATP release. Parameter values as in Fig. 2, except for $a'_d = 0.41$. Initial conditions as in Appendix E.

These results suggest that our finding from the bifurcation analysis, that calcium mediated cell cycle acceleration is unlikely to account for a significant increase in cellular proliferation, is robust for our model.

We conclude our analysis by first discussing and then demonstrating that cell cycle recruitment of a quiescent cell by a proliferating cell via an ATP mediated calcium signalling mechanism is viable and this could be the dominant mechanism by which calcium increases proliferation rates. In order to describe, in detail, how this is achieved, we refer to the bifurcation diagrams in Fig. 2 (a and b). In this figure the cell cycle dynamics of the ATP blocked case (red symbols) are equivalent to the dynamics of the original cell cycle model of Obeyesekere et al., which exhibits an area of multistability where limit cycle solutions and fixed point solutions coexist. Obeyesekere et al. (1999) showed that, whilst keeping parameter values fixed, increasing the Cyclin E concentration can stop a cell from cycling by driving the system from the branch of limit cycle solutions to the fixed point solution branch. Clearly, the converse is also true, i.e. it is possible to drive a cell from the branch of fixed point solutions to the branch of high amplitude limit cycle solutions, for example by changing the Cyclin D concentration. Moreover, Fig. 2 shows that ATP mediated calcium signalling acts to increase the area of multistability. This has important biological implications in that it suggests that ATP mediated calcium-cell cycle coupling can make cells more susceptible to cycling. In particular, cells can cycle for values of a'_d for which they would not in the absence of ATP mediated calcium signalling. For example, for the Cyclin D dependent model variant (Fig. 2(a)), high amplitude stable limit cycle solutions exist for $0.385 < a'_d < 0.395$, but do not exist for these value in the absence of coupling. Similarly, for the R_s dependent model (Fig. 2(b)), limit cycle solutions exist for $0.345 < a'_d < 0.395$, but vanish when ATP mediated calcium coupling is switched off. We believe that the area of multistability is relevant to the process of a cycling radial glial cell inducing a quiescent cell into G_1 phase of the cell cycle via ATP mediated calcium signals. In particular, let us consider a multicellular model. Quiescent cells would have initial conditions such that they sit on the stable fixed point solution branch within the area of multistability. A cycling cell, whose initial conditions are such that it sits on the high amplitude limit cycle branch, may be able to recruit quiescent cells to which it is coupled on to the upper limit cycle branch. Recruitment would be facilitated via the release of ATP from the cycling cell which would induce calcium release in the quiescent cells. Calcium elevations in the quiescent cells would, in turn, lead to an increase in Cyclin D activity which could sweep the cells up onto the high amplitude branch of limit cycle solutions.

We demonstrate the viability of this scenario in Fig. 8 which shows simulations for systems of two cells in which extracellular ATP is allowed to diffuse through extracellular space according to

$$\frac{d[\mathrm{ATP}_{\mathrm{E},1}]}{dt} = ATP_{rel,1} - ATP_{deg,1} + D_{ATP}([\mathrm{ATP}_{\mathrm{E},2}] - [\mathrm{ATP}_{\mathrm{E},1}]), \tag{16}$$

$$\frac{d[\mathrm{ATP}_{\mathrm{E},2}]}{dt} = ATP_{rel,2} - ATP_{deg,2} + D_{ATP}([\mathrm{ATP}_{\mathrm{E},1}] - [\mathrm{ATP}_{\mathrm{E},2}]), \tag{17}$$

where subscripts indicate the cell number and D_{ATP} is a diffusion parameter. Parameter values are chosen such that both cells lie within the area of multistability for the single cell model for the ATP coupled case, but outside the area of multistability for the ATP blocked case. Two scenarios are considered for both model variants. In the first, ATP mediated calcium coupling is enabled

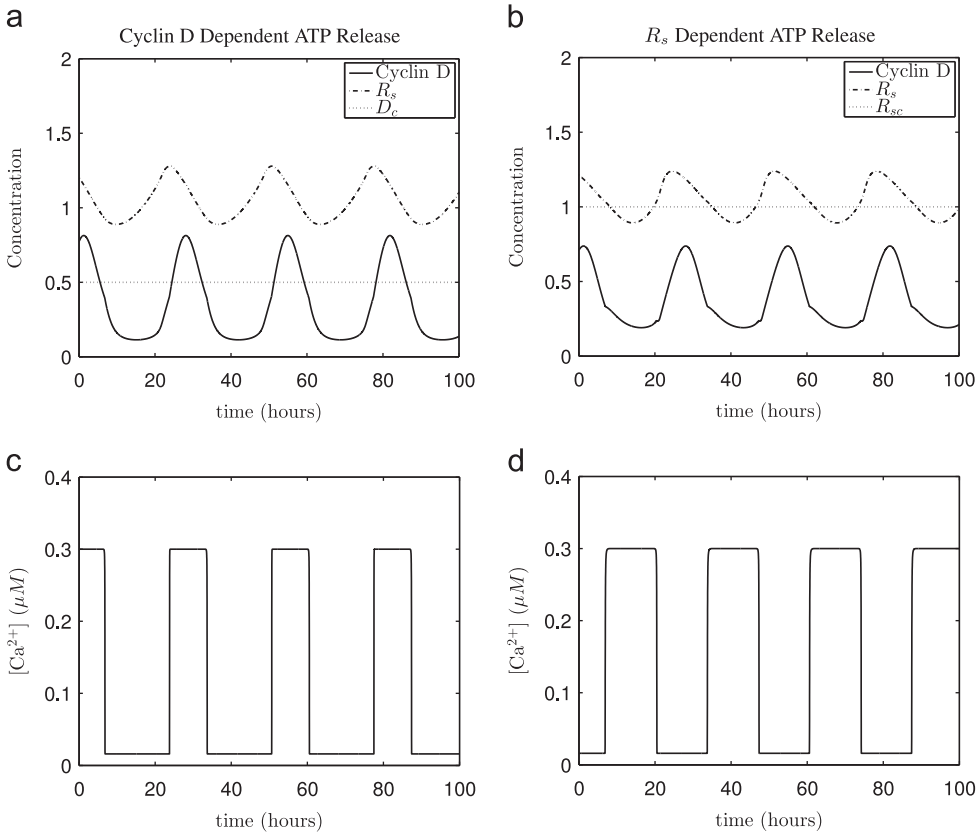

Fig. 5. An example demonstrating the nonlinear effect of calcium. Despite calcium release of different durations, because of the different times during the cell cycle at which release occurs, the impact on the cell cycle period is identical. (a, c) correspond to the Cyclin D dependent release model and (b, d) to the R_s dependent ATP release model. The cell cycle period for both model variants is 26.9 h, yet the duration of calcium release is longer for the R_s dependent ATP release model (cf. (c) with (d)). Parameter values as in Tables D1–D3 except for $D_c = 0.433$. Initial conditions as in Appendix E.

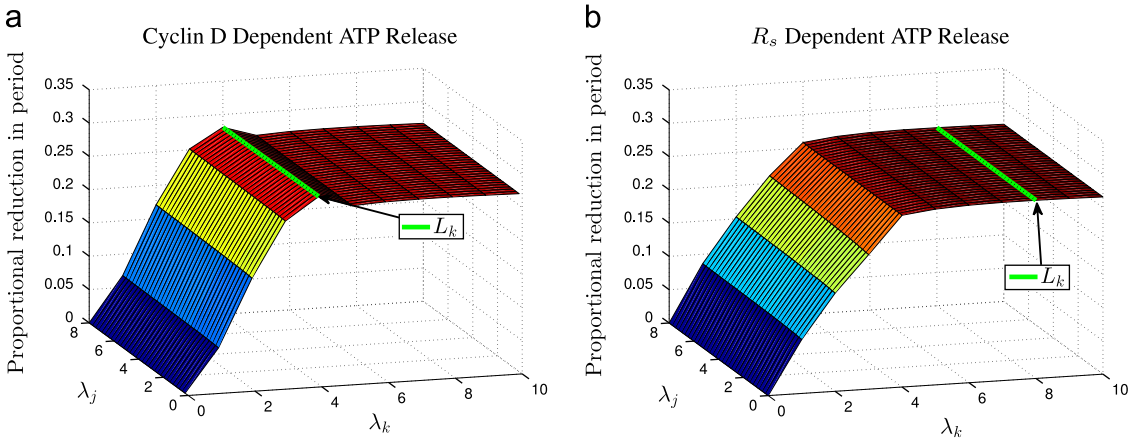

Fig. 6. Proportional reduction in cell cycle period as a function of λ_j and λ_k. The maximum proportional reduction, for each value of λ_j, brought about by changes in λ_k is indicated by the solid green line. $P_j = K_{deg}$ and $P_k = \gamma$. $\lambda_k \in [0, 10]$ and $\lambda_j \in [0, 8]$ were both sampled at regular intervals of 0.25. Baseline parameter values given in Tables D1–D3. (For interpretation of the references to colour in the text, the reader is referred to the web version of this paper.)

whilst in the second ATP mediated calcium coupling is disabled. In all cases, the initial conditions of one cell (the 'driving cell') are chosen such that it will oscillate in isolation when calcium-cell cycle coupling is enabled, while the initial conditions of the second cell (the 'quiescent cell') are chosen to lie on the stable fixed point branch of the single cell model. It is clear that for the case with ATP mediated calcium-cell cycle coupling (Fig. 8(a and b)), that the quiescent cell is recruited onto the oscillatory regime by the driving cell. While for the uncoupled case (c,d) the oscillations in the driving cell eventually die out, with both cells eventually exhibiting stable fixed point solutions.

4. Discussion

In this paper, in order to answer the question of how ATP mediated calcium signals increase radial glia proliferation, we formed a model for coupled calcium-cell cycle dynamics in a single radial glial cell. Although it has not been experimentally determined precisely how intracellular calcium regulates proliferation rates in radial glia, studies on other cell types indicate that calcium, alone or as part of a complex, can cause an increase in proliferation rates by either accelerating G_1 and reducing the overall cell cycle period (Rasmussen and Means, 1987, 1989) or

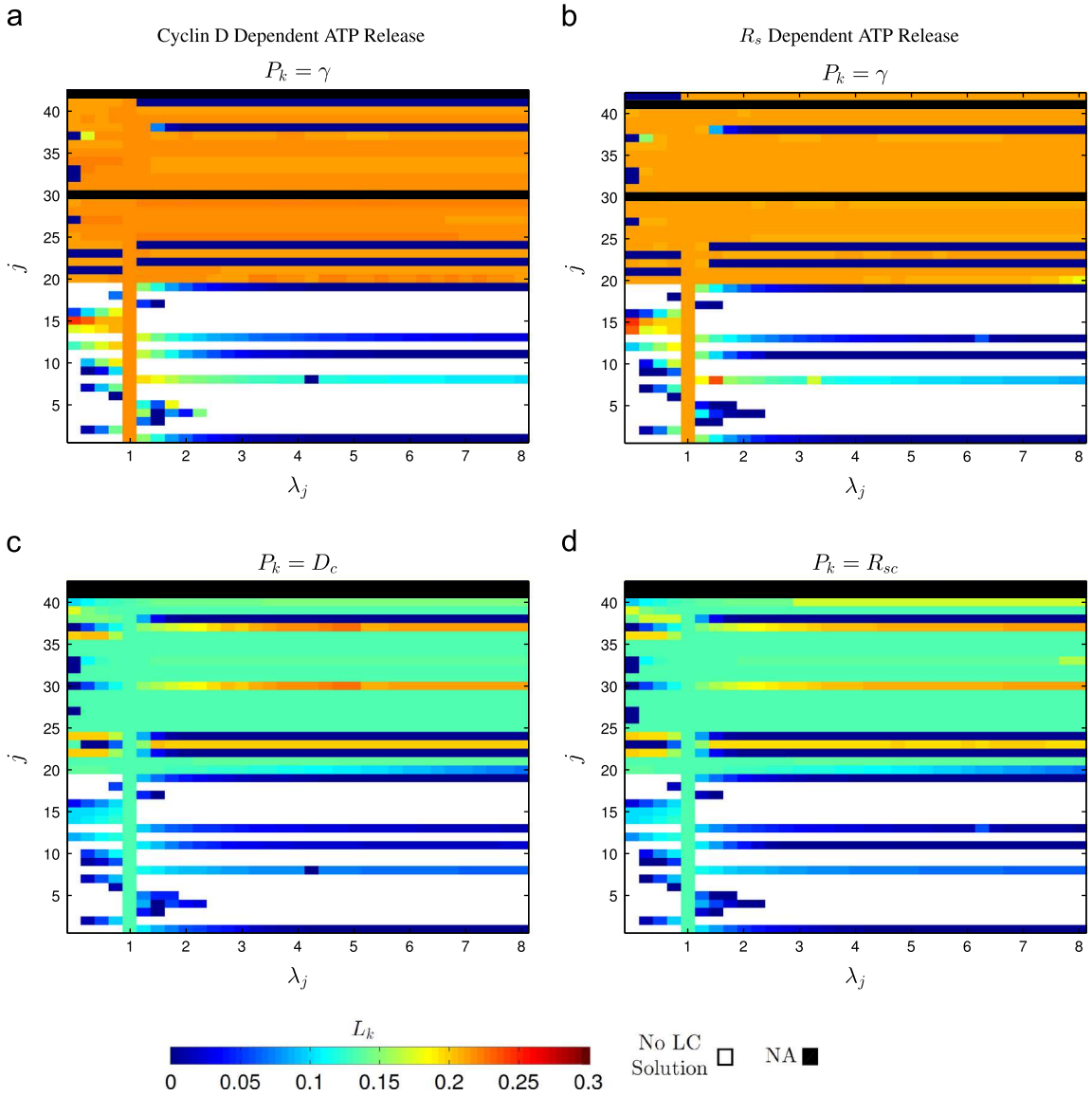

Fig. 7. Numerical results indicating that, for all parameter regimes, the cell cycle period remains weakly dependent on the calcium coupling strength γ and ATP release thresholds D_c and R_{sc}. The colours in the heat maps correspond to the maximum proportional reduction in cell cycle period L_k brought about by changes in control parameters. The control parameter $P_k = \gamma$ in (a,b) while the thresholds D_c and R_{sc} are chosen as P_k in (c,d). White in the heat maps corresponding to parameter regimes for which there are no limit cycle (LC) solutions. Black corresponds to the instances where a value for L_k cannot be calculated either because $j=k$ or the parameter indexed by j is not included in the particular model variant. In all figures, $\lambda_j \in [0, 8]$ was sampled at regular intervals of 0.25. In (a,b), $\lambda_k \in [0, 10]$ was sampled at regular intervals of 0.25, in (c) $\lambda_k \in [0, 0.7]$ was sampled at regular intervals of 0.1 and in (d) $\lambda_k \in [0.8, 1.4]$ was sampled at regular at intervals of 0.1. The ranges for the fold change parameter λ_k were chosen as previous results indicate the cell cycle period has a local minimum or reaches an asymptotic value within them (see Fig. 3). Parameter indices and baseline values given in Tables D1–D3. (For interpretation of the references to colour in this figure caption, the reader is referred to the web version of this paper.)

inducing cells, which would otherwise lie dormant in the quiescent G_0 state, to embark on the cell cycle (Hazelton et al., 1979; Whitfield et al., 1979; Boynton et al., 1976). From the results of Section 3 we infer that, for our model, the reduction in the cell cycle period brought about by ATP mediated calcium release is modest (approximately 10% for realistic parameter regimes). In order to obtain an increase in the proliferation rate of 82.8% as obtained from Weissman et al. (2004), a reduction in period close to 45.3% is required. This suggests that the modulation of the frequency of oscillation caused by calcium plays a minor role with regard to accounting for the large increase in cellular proliferation brought about by calcium signalling. Crucially however our bifurcation results reveal a region of multistability that is extended by the calcium coupling. This result and simulations of two cell systems are consistent with the notion that a proliferating cell may induce oscillations in otherwise quiescent cells via a calcium signalling mechanism. The actual increase in the proliferation rate will depend on the proportion of cells that would otherwise lie dormant in the absence of ATP mediated calcium waves, but such a cell-cycle recruitment mechanism could in principle account for the 82.8% increase in proliferation and it may be predominantly by these means that calcium acts to increase overall cellular proliferation in radial glia.

To keep our model tractable, we used a low dimensional model for the cell cycle. An interesting avenue of future investigation would be to consider whether the inclusion of a more biophysically realistic cell cycle model (such as that of Novak and Tyson, 2004; Swat et al., 2004; Gérard and Goldbeter, 2011 or Pfeuty, 2012) would lead to results consistent with those presented in this paper. We note from Fig. S1 of Pfeuty (2012) that this model has structural similarities to our model in that an area of bistability in which two steady state solutions (one of which corresponds to the

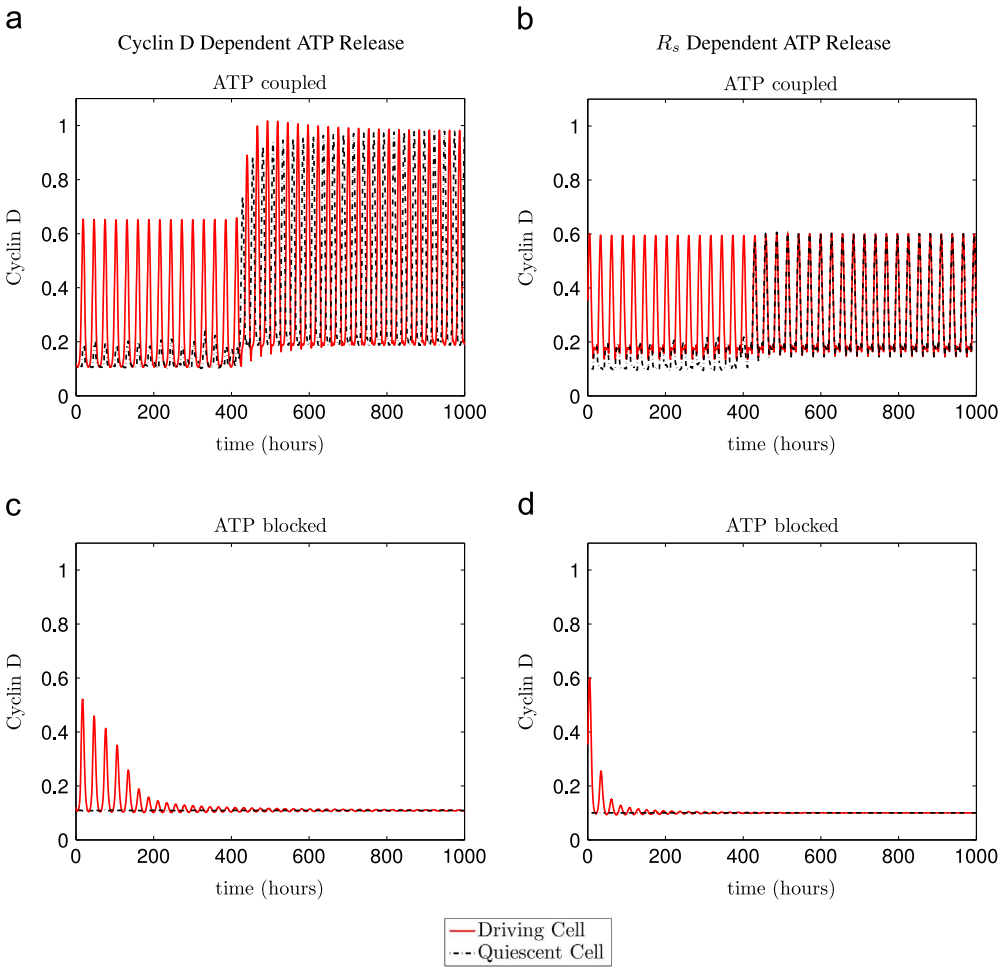

Fig. 8. (a,b) Illustrative example of how, in a system of two coupled cells, a driving cell may recruit a quiescent cell onto the cell cycle. (c,d) demonstrate that when ATP mediated-calcium coupling is disabled (i.e. $[ATP_E]=0$) recruitment fails and oscillations in the driving cell die out. Parameter values as in Tables D1–D3 except for $D_{ATP}=0.5\ \mu M^{-1}s^{-1}$, $a_d'=0.39$ for (a,c) and $a_d'=0.36$ for (b,d). Initial conditions as in Appendix E.

S phase proliferative state and the other to the quiescent state) coexist for a range of values for a parameter which controls the Cyclin D synthesis. This is comparable to the area of multistability in our model in which limit cycle solutions (corresponding to the proliferative state) and fixed point solutions (corresponding to the quiescent state) coexist (see Fig. 2). For our model this area plays a crucial role in allowing for a driving cell to recruit quiescent cells. It is conceivable therefore that in the model of Pfeuty (2012), the area of bistability could permit similar behaviour and allow for recruitment of a quiescent cell by a driving cell. The model of Gérard and Goldbeter also exhibits an area of bistability (see Fig. 8 (d) of Gérard and Goldbeter, 2011) where low amplitude limit cycle and high amplitude limit cycle solutions coexist, again for a range of values for a parameter which controls the Cyclin D synthesis. Here also, it is conceivable that a cell on the high amplitude limit cycle branch could lift a non-proliferating cell sat on the branch of low amplitude limit cycle solutions up into the proliferative regime via ATP mediated calcium signals.

In this study we did not consider the impact of calcium on Cdc25 and Cdk1. As calcium affects these proteins either at the G_2/M transition or during M phase, we expect that the inclusion of these pathways will have little or no impact on our result that ATP mediated calcium release can lift a cell out of G_0 and into G_1. By incorporating these pathways into our model, we may find that calcium acts to accelerate M phase entry and/or progression of an already cycling cell, leading to a reduction in period. However, our results suggest that this reduction is very likely to be modest and, in itself, is highly unlikely to account for the experimentally observed increase in proliferation rates.

Our work focuses on non-differentiating cells. The changes that occur in cell cycle behaviour of differentiating radial glia are complex (see Patten et al., 2003 for example) and incorporating such changes into a model would provide an interesting avenue for future research. Other future work will also investigate in more detail whether radial glia cell cycle recruitment can account for the increased proliferation rates discovered by Weissman et al. (2004). It will be important to consider multicellular systems and investigate whether, and under what conditions, cycling cells can induce dormant cells to cycle and the impact of this on overall cellular proliferation. We note that there may be significant variation in parameters within a population of cells and it will be important to consider, for example, whether an intrinsically cycling cell can recruit one that, in isolation, cannot oscillate. It has also been hypothesised that the calcium signalling mechanism enables the synchronisation of the cell cycles of clusters of radial glial cells, leading to the shedding of daughter cells in uniform sheets (Weissman et al., 2004). This concept will be tested in future work.

Appendix A. Modelling calcium release

The model of Li and Rinzel for calcium release (Li and Rinzel, 1994) which Bennett et al. incorporate into their model for ATP

mediated calcium release in astrocytes is given by

$$\frac{d[Ca^{2+}]}{dt} = \mu(J_{ER}^{out} - J_{ER}^{in}), \tag{A.1}$$

$$\frac{dh}{dt} = A[K_d - ([Ca^{2+}] + K_d)h], \tag{A.2}$$

$$J_{ER}^{out} = \left[L + \frac{P_{IP3R}[IP_3]^3[Ca^{2+}]^3h^3}{([IP_3]+K_i)^3([Ca^{2+}]+K_a)^3}\right]([Ca^{2+}]_{ER} - [Ca^{2+}]), \tag{A.3}$$

$$J_{ER}^{in} = \frac{V_{SERCA}[Ca^{2+}]^2}{[Ca^{2+}]^2 + K_{SERCA}^2}, \tag{A.4}$$

$$[Ca^{2+}]_{ER} = \frac{C_t - [Ca^{2+}]}{\sigma}. \tag{A.5}$$

In the model (A.1)–(A.5), C_t is the total calcium (assumed to be constant) and it is composed of calcium in the ER ($[Ca^{2+}]_{ER}$) and calcium in the cytosol ($[Ca^{2+}]$). In Eq. (A.1) μ describes calcium buffering. Calcium release, triggered by IP_3, is controlled by the flux of calcium from the ER into the cytosol (J_{ER}^{out}, Eq. (A.3)) and the flux from the cytosol into the ER (J_{ER}^{in}, Eq. (A.4)). The flux into the cytosol depends upon a gating variable (h, Eq. (A.2)), which is the fraction of ion channels available to open. L and P_{IP3R} are the ER leak permeability and the maximum total permeability of IP_3 channels respectively. V_{SERCA} is the maximum pump rate of calcium into the ER and K_{SERCA} is a constant which represents the calcium concentration at which the SERCA pump reaches half maximal efficiency. K_d, K_i, and K_a are dissociation constants. Under certain parameter regimes, system (A.1)–(A.5) exhibits oscillatory solutions.

The calcium dynamics described by Eqs. (A.1)–(A.5) and the cell cycle dynamics of our model occur over very different timescales; the former has a period of oscillation of seconds and the latter hours. We wish to investigate the effect calcium has on the radial glial cell cycle. Therefore it is natural to replace oscillatory calcium release defined in Eqs. (A.1)–(A.5) with time averaged calcium release defined in Eq. (15). Using the non-linear least squares Marquardt–Levenberg algorithm (Marquardt, 1963) we fitted Eq. (15) to data for the average calcium concentration as a function of IP_3. The data was obtained via numerical continuation of steady state and limit cycle solutions of the Li and Rinzel model. In the absence of specific knowledge of the spiking profile of calcium in radial glia, to generate the data from the model of Li and Rinzel we used the parameter values of Fall et al. (2002). Such values ensure that key features of calcium release, universally present in many cell types (Fall et al., 2002), are expressed. These features include the maximum and minimum calcium amplitude being independent of the concentration of IP_3 and the oscillatory period of calcium being a decreasing function of IP_3. Average calcium as a function of IP_3 for the model of Li and Rinzel is plotted in Fig. A1 together with Eq. (15). For values of IP_3 less than approximately 1.25 μM, the fit is very good. For all parameter regimes considered in this paper, IP_3 concentrations never exceed 1.25 μM. Hence, even though the fit is not so good for larger values of IP_3, this will not significantly affect results.

To confirm that replacing the model of Li and Rinzel with function (15) describing calcium release does not affect the results of this work, we simulated our ATP coupled model (i.e. with ATP mediated calcium-cell cycle coupling) using the model of Li and Rinzel for calcium release (which we refer to as the 'full' model) as well as also simulating the ATP coupled case but using approximated calcium dynamics given by Eq. (15) (which we refer to as the 'reduced' model). Results using parameter regimes, in which parameter values other than the calcium parameters are varied, confirm that the system with time averaged calcium release is in excellent agreement with the model in which the model of Li and Rinzel was used. Moreover, the reduced model results in an 8-fold saving on computation time. A representative example illustrating the very good agreement between the full and reduced models is given in Fig. A2. In this case, for the Cyclin D (R_s) dependent ATP release model, the duration of calcium release for one cell cycle for the reduced model is only approximately 0.327% (0.491%) greater than for the full model and the cell cycle period for the reduced model is approximately 0.0505% (0.102%) less than the period of the full model.

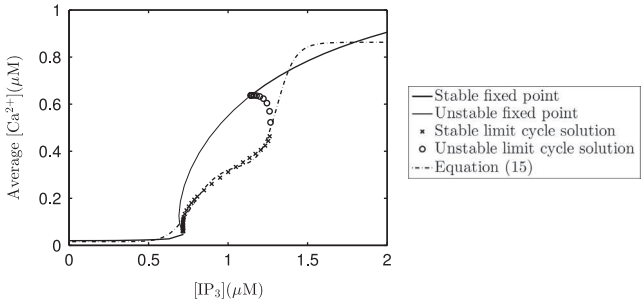

Fig. A1. Bifurcation diagram for the Li and Rinzel model for IP_3 mediated calcium release (Eqs. (A.1)–(A.5)), showing which values of the parameter $[IP_3]$ give rise to calcium oscillations. For comparison the time averaged function for calcium release defined in Eq. (15) is also shown. Parameter values given in Tables D1–D3 and by $\mu = 0.0025$ pL^{-1} $L = 1332$ pL h^{-1}, $P_{IP3R} = 95,904,000$ pL h^{-1}, $K_i = 1.0$ μM, $K_a = 0.4$ μM, $V_{SERCA} = 1,440,000$ aMol h^{-1}, $K_{SERCA} = 0.2$ μM, $A = 1800$ h^{-1}, $K_d = 0.4$ μM, $\sigma = 0.185$, and $[Ca^{2+}]_T = 2$ μM.

We note that calcium oscillations of different frequencies can have different effects on cellular dynamics (Dolmetsch et al., 1998; Thul et al., 2008) and that by simplifying the calcium release equations as described in this section we cannot investigate how the frequency of calcium oscillations will affect the cell cycle. Therefore, to confirm that frequency coding has no effect on the coupling of the cell cycle, we introduce a scale factor S_F into Eqs. (A.1) and (A.2) as

$$\frac{d[Ca^{2+}]}{dt} = S_F(\mu(J_{ER}^{out} - J_{ER}^{in})), \tag{A.6}$$

$$\frac{dh}{dt} = S_F(A[K_d - ([Ca^{2+}] + K_d)h)]. \tag{A.7}$$

By varying S_F different frequencies for calcium oscillations can be imposed into the system. In Fig. A3, we show the results of two simulations, one where $S_F = 0.11$ and on in which $S_F = 0.31$. The evolution of Cyclin D is identical in both cases even though the frequency of calcium oscillations of the two instances is different. The Pearson's r linear correlation coefficient (Lee Rodgers and Nicewander, 1988) between the Cyclin D values for the two cases in Fig. A3 is 1, confirming that they are identical. In Table A1 we give the Pearson's r values for the values of Cyclin D obtained from simulations using 11 different values for the scale factor parameter S_F. In every case, the coefficient is either 1 or almost 1 confirming that the values for Cyclin D are identical in each simulation and that a frequency coding mechanism has no effect on the coupling.

Appendix B. Model equations

Below we reproduce Eqs. (1)–(15) which make up our model for ATP mediated calcium-cell cycle coupling for a single radial glial cell

$$\frac{dD}{dt} = a_d \cdot GF - d_D ED,$$

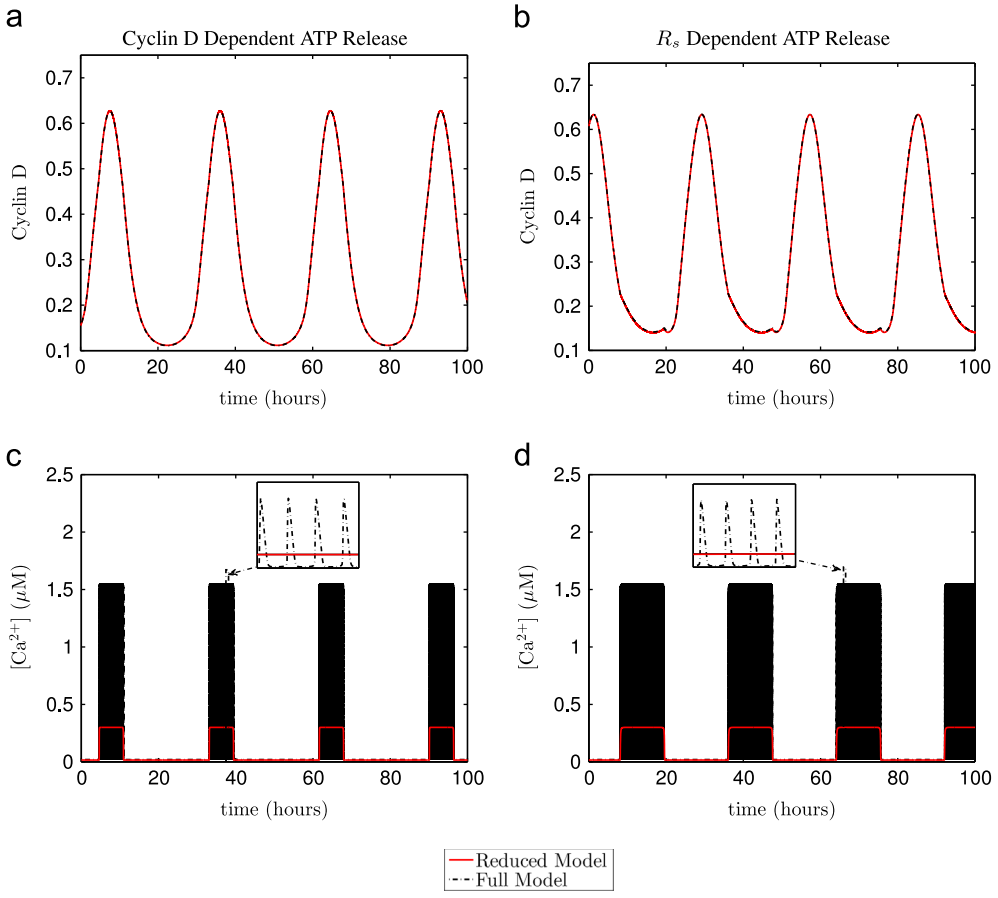

Fig. A2. Simulations in which ATP mediated calcium release is coupled to the cell cycle dynamics in a single radial glia cell (system (1)–(14)) using time averaged calcium dynamics (Eq. (15), solid red lines, the 'reduced model') and with the calcium release model of Li and Rinzel (Eqs. (A.1)–(A.5), black dot-dashed lines, the 'full model'). The first column of plots correspond to the Cyclin D dependent ATP release model variant ($(i_1, i_2) = (D, D_c)$) and the second column to the R_s dependent ATP release model variant ($(i_1, i_2) = (R_{sc}, R_s)$). In (a,b) the match between the reduced model and the full model is excellent. Note, in all plots the solution trajectories for the reduced and full models are superimposed on each other. The insets of (c,d) show oscillatory calcium dynamics in the full model in detail. Initial conditions as for Appendix E. Parameter values as for Tables D1–D3 except for $\gamma = 0.4\,\mu M^{-1}\,h^{-1}$. (For interpretation of the references to colour in this figure caption, the reader is referred to the web version of this paper.)

$$\frac{dE}{dt} = a_E(1 + a_f(E2F_T - R_s)) - d_E X E,$$

$$\frac{dR}{dt} = \frac{p_X(R_T - R_s - R)X}{q_X + (R_T - R_s - R) + X} - p_s(E2F_T - R_s)R,$$

$$\frac{dR_s}{dt} = p_s(E2F_T - R_s)R - \frac{p_D R_s D}{q_D + R_s + D} - \frac{p_E R_s E}{q_E + R_s + E},$$

$$\frac{dX}{dt} = a_X E + \beta(E2F_T - R_s) + gX^2 E - d_X X,$$

$$a_d([Ca^{2+}]) = a_d' + \gamma([Ca^{2+}] - [Ca^{2+}]_b), \quad \rho = \frac{[ATP_E]}{K_R + [ATP_E]},$$

$$G^* = \frac{\rho + \nu}{K_G + \rho + \nu}, \quad \frac{d[IP_3]}{dt} = r_h^* G^* - k_{deg}[IP_3],$$

$$\frac{d[ATP_I]}{dt} = ATP_{prod} - ATP_{rel}, \quad \frac{d[ATP_E]}{dt} = ATP_{rel} - ATP_{deg},$$

$$ATP_{prod} = \alpha([ATP_I]_{max} - [ATP_I]), \quad ATP_{deg} = V_{deg}\frac{[ATP_E]}{K_{deg} + [ATP_E]},$$

$$ATP_{rel} = \left(\frac{[IP_3] - [IP_3]_{min}}{K_{rel} + [IP_3]}\right) V_{ATP}([ATP_I] - [ATP_E]) \times T(i_1 - i_2) T([IP_3] - [IP_3]_{min}),$$

$$T(x) = \frac{1}{2}\left(\tanh\left(\frac{x}{\varepsilon}\right) + 1\right), \quad [Ca^{2+}] = [Ca^{2+}]_b + \frac{p_1[IP_3]^m}{p_2^m + [IP_3]^m} + \frac{p_3[IP_3]^n}{p_4^n + [IP_3]^n}.$$

For the Cyclin D dependent ATP release model variant $(i_1, i_2) = (D, D_c)$ and for the R_s dependent ATP release model variant $(i_1, i_2) = (R_{sc}, R_s)$.

Appendix C. Wiring diagram of model variables

Schematic illustration of the positive and negative interactions between the model variables given by Eqs. (1)–(15) is shown in Fig. C1.

Appendix D. Choice of parameter values

We have, where appropriate, used parameter values from the original component models, with a few exceptions that we discuss here. In the original model of Bennett et al. (2005) cells are regarded as three-dimensional cubes with proteins secreted and absorbed via two-dimensional cell walls. For simplicity, in our model we consider cells as point sources. Consequently it is necessary to change the values for r_h^*, k_{deg} and V_{ATP} given in Bennett et al. (2005) in order to obtain behaviour which closely mimics the case where cells are modelled as three-dimensional cubes. We arrived at appropriate values by simulating our model under different parameter regimes and comparing these results to numerical simulation results provided in Bennett et al. (2005). For the parameters that govern ATP degradation (V_{deg} and K_{deg}), different values for different cell types have been published in the biological literature. Gordon et al. (1989) derived values of $K_{deg} = 221\,\mu M$ and $V_{deg} = 9000\,\mu M\,h^{-1}$ for arterial muscle cells of pigs. It is important to note however that ATP degradation depends heavily upon cell type as well as cellular concentration.

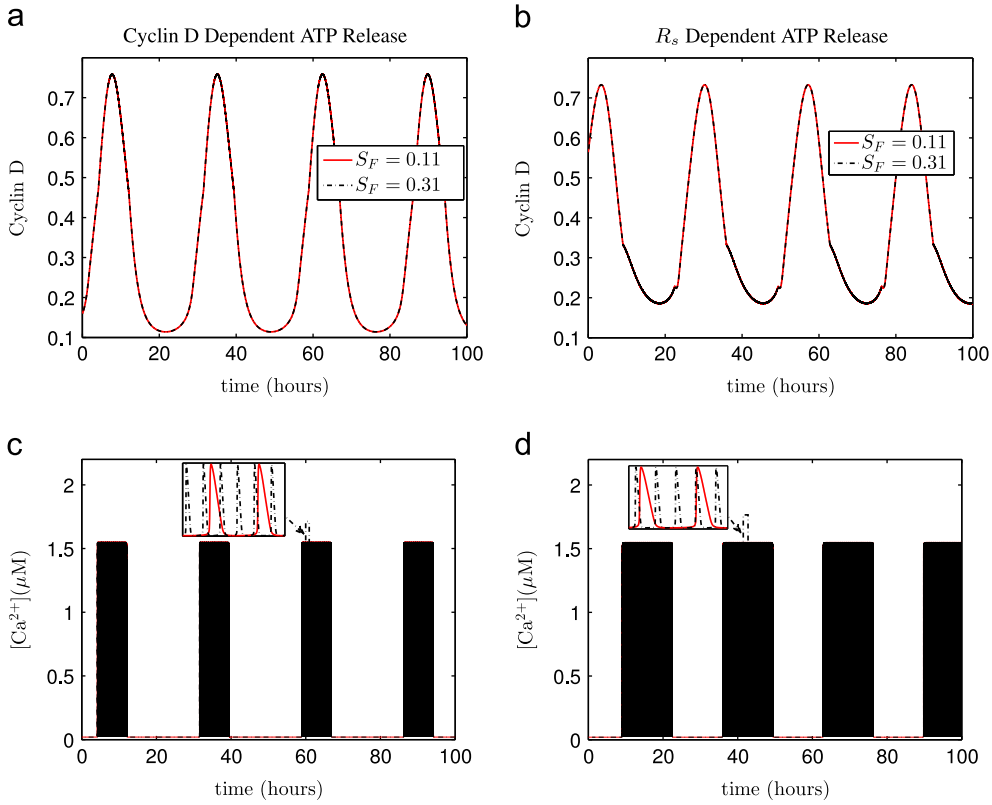

Fig. A3. Example illustrating that changes in the frequency of calcium oscillations have no effect on the cell cycle. (a,b) show the evolution of Cyclin D for two different values of the scale factor parameter S_F which effectively controls the frequency of calcium oscillations for the Li and Rinzel model. (c,d) show the calcium oscillations with the insets of these plots illustrating the different oscillatory frequencies of the two cases. Simulations obtained by integrating system (1)–(14) with the modified version of the calcium release model of Li and Rinzel which permits frequency modulations (Eqs. (A.3)–(A.5), (A.6) and (A.7)). Initial conditions as for Appendix E. Parameter values as for Tables D1–D3, and in the figure.

Table A1
Pearson's correlation scores for Cyclin D values obtained from simulations in which different values for S_F were used.

S_F	**0.01**	**0.11**	**0.21**	**0.31**	**0.41**	**0.51**	**0.61**	**0.71**	**0.81**	**0.91**	**1**
Cyclin D dependent ATP release											
0.01	1.0000	–	–	–	–	–	–	–	–	–	–
0.11	0.9997	1.0000	–	–	–	–	–	–	–	–	–
0.21	0.9997	1.0000	1.0000	–	–	–	–	–	–	–	–
0.31	0.9997	1.0000	1.0000	1.0000	–	–	–	–	–	–	–
0.41	0.9997	1.0000	1.0000	1.0000	1.0000	–	–	–	–	–	–
0.51	0.9997	1.0000	1.0000	1.0000	1.0000	1.0000	–	–	–	–	–
0.61	0.9997	1.0000	1.0000	1.0000	1.0000	1.0000	1.0000	–	–	–	–
0.71	0.9997	1.0000	1.0000	1.0000	1.0000	1.0000	1.0000	1.0000	–	–	–
0.81	0.9997	1.0000	1.0000	1.0000	1.0000	1.0000	1.0000	1.0000	1.0000	–	–
0.91	0.9996	1.0000	1.0000	1.0000	1.0000	1.0000	1.0000	1.0000	1.0000	1.0000	–
0.1	0.9996	1.0000	1.0000	1.0000	1.0000	1.0000	1.0000	1.0000	1.0000	1.0000	1.0000
R_s dependent ATP release											
0.01	1.0000	–	–	–	–	–	–	–	–	–	–
0.11	0.9997	1.0000	–	–	–	–	–	–	–	–	–
0.21	0.9997	1.0000	1.0000	–	–	–	–	–	–	–	–
0.31	0.9997	1.0000	1.0000	1.0000	–	–	–	–	–	–	–
0.41	0.9997	1.0000	1.0000	1.0000	1.0000	–	–	–	–	–	–
0.51	0.9997	1.0000	1.0000	1.0000	1.0000	1.0000	–	–	–	–	–
0.61	0.9997	1.0000	1.0000	1.0000	1.0000	1.0000	1.0000	–	–	–	–
0.71	0.9997	1.0000	1.0000	1.0000	1.0000	1.0000	1.0000	1.0000	–	–	–
0.81	0.9997	1.0000	1.0000	1.0000	1.0000	1.0000	1.0000	1.0000	1.0000	–	–
0.91	0.9997	1.0000	1.0000	1.0000	1.0000	1.0000	1.0000	1.0000	1.0000	1.0000	–
0.1	0.9997	1.0000	1.0000	1.0000	1.0000	1.0000	1.0000	1.0000	1.0000	1.0000	1.0000

ATP is degraded into adenosine diphosphate (ADP) by ecto-nucleotidases present on the extracellular surface of cells (Joseph et al., 2004; Reigada et al., 2005). As different cell types express different ecto-nucleotidases in different proportions, the ability of different cells to degrade extracellular ATP will differ also. Joseph et al. (2004) investigated ATP degradation by astrocytes, and their results are at odds with those of Gordon et al. By fitting the data published in the paper of Joseph et al. (2004) to the model we

use for ATP degradation ($d[\mathrm{ATP_E}]/dt = -V_{deg}[\mathrm{ATP_E}]/(K_{deg}+[\mathrm{ATP_E}])$, see Eq. (12)), we derived values for $V_{deg} = 21.33\ \mu\mathrm{M\ h^{-1}}$ and $K_{deg} = 5.1434\ \mu\mathrm{M}$ (results plotted in Fig. D1).

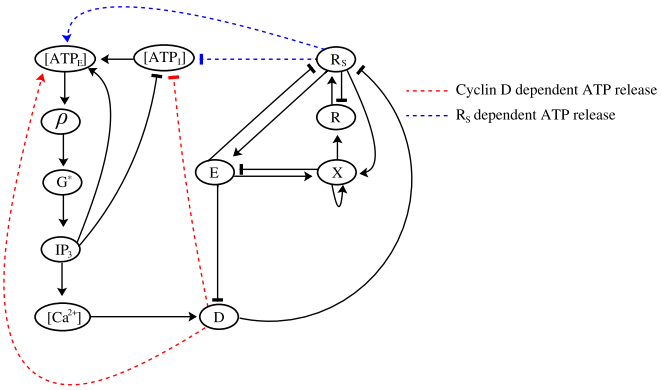

Fig. C1. Schematic illustration of the positive and negative interactions between the model variables given by Eqs. (1)–(15).

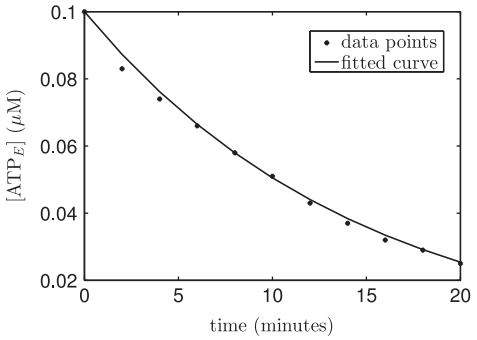

Fig. D1. Experimental data of Joseph et al. (2004) showing how an initial ATP concentration of 0.1 μM degrades over time and a simulated ATP degradation curve. The data was fitted to the model for ATP degradation given by Eq. (12) using the unconstrained nonlinear optimisation method of Lagarias et al. (1999).

As radial glial cells bear a closer cellular resemblance to the astrocytes that Joseph et al. studied than to the pig cells that Gordon et al. studied, it seems reasonable to choose values of V_{deg} and K_{deg} skewed more towards the results of Joseph et al. (2004). However, it is also important to note that Joseph et al. considered relatively small concentrations of ATP in their experiments ($\sim 0.1\ \mu\mathrm{M}$) and their results may not hold as well for larger ATP concentrations. Bearing in mind that in this paper we consider ATP concentrations of orders of magnitude greater than this, we should therefore not totally dismiss the results of Gordon et al. (1989) as they consider similarly large concentrations of ATP in their experiments. We therefore regard $K_{deg} = 50\ \mu\mathrm{M}$ and $V_{deg} \in [36, 7200]\ \mu\mathrm{M\ h^{-1}}$ as physically realistic values.

Guthrie et al. (1999) suggest that a value of 5000 μM represents a plausible, but likely very high estimate for cytosolic ATP concentration in astrocytes. We therefore consider values of 500 μM for $[\mathrm{ATP_I}]_{max}$, which represents the maximum intracellular ATP concentration. For simplicity, and in the absence of evidence to the contrary, we assume that internal ATP stores of radial glia never fully deplete, even with open hemichannels. To ensure this we take a value for ATP production strength α which guarantees that, when hemichannels are open, ATP production exceeds ATP release.

We vary the parameter γ which controls the calcium coupling strength in our analysis in order to investigate its effect upon our model. We set the critical values D_c and R_{sc} so that ATP release occurs at the appropriate point during the cell cycle (see Section 2 for details).

The period of the mammalian radial glial cell cycle ranges from approximately 8–18 h in mice (Takahashi et al., 1995) to 22–55 h in primates (Kornack and Rakic, 1998). The cell cycle model of Obeyesekere et al. has non-dimensional time units and for the baseline parameter values in our radial glial cell model the cell cycle period is 27.29 for the Cyclin D dependent ATP release variant and 26.85 for R_s ATP release model variant. We therefore introduce dimensional time such that 1 unit of dimensionless time equals 1 h, giving cell cycle times consistent with the above biological observations. For the model of Bennett et al. (2005) we rescale time from seconds to hours for compatibility with the cell cycle model. All parameter values used in our models are given in Tables D1–D3.

Table D1
Parameter values for Obeyesekere et al. cell cycle model.

Index	Parameter	Value	Source	Description
1	GF	0.25384	Obeyesekere et al. (1999)	Growth factor activity
2	d_D	$0.4\ \mathrm{h^{-1}}$	Obeyesekere et al. (1999)	Rate parameter at with which Cyclin D is degraded by active Cyclin E/Cdk2
3	a_E	$0.16\ \mathrm{h^{-1}}$	Obeyesekere et al. (1999)	E2F independent Cyclin E synthesis rate parameter
4	a_f	0.9	Obeyesekere et al. (1999)	E2F dependent Cyclin E synthesis rate parameter
5	$E2F_T$	1.5	Obeyesekere et al. (1999)	Total E2F concentration
6	d_E	$0.2\ \mathrm{h^{-1}}$	Obeyesekere et al. (1999)	Rate parameter at with Cyclin E is degraded by the CPI
7	p_X	$0.48\ \mathrm{h^{-1}}$	Obeyesekere et al. (1999)	Rate parameter at with which the CPI dephosphorylates RB
8	q_X	$0.8\ \mathrm{h^{-1}}$	Obeyesekere et al. (1999)	Michaelis constant
9	R_T	2.5	Obeyesekere et al. (1999)	Total RB
10	p_s	$0.6\ \mathrm{h^{-1}}$	Obeyesekere et al. (1999)	Constant at which free unphosphorylated RB sequesters E2F
11	p_D	$0.48\ \mathrm{h^{-1}}$	Obeyesekere et al. (1999)	Rate parameter at which active Cyclin D/Cdk4 phosphorylates RB
12	q_D	$0.6\ \mathrm{h^{-1}}$	Obeyesekere et al. (1999)	Michaelis constant
13	p_E	$0.096\ \mathrm{h^{-1}}$	Obeyesekere et al. (1999)	Rate parameter at which Cyclin E phosphorylates RB
14	q_E	$0.6\ \mathrm{h^{-1}}$	Obeyesekere et al. (1999)	Michaelis constant
15	a_X	$0.08\ \mathrm{h^{-1}}$	Obeyesekere et al. (1999)	Rate parameter of Cyclin E/Cdk2 dependent CPI production
16	β	$0.2\ \mathrm{h^{-1}}$	Obeyesekere et al. (1999)	Rate parameter of free E2F dependent CPI production
17	g	$0.528\ \mathrm{h^{-1}}$	Obeyesekere et al. (1999)	CPI autocatalytic reaction rate parameter
18	d_X	$1.04\ \mathrm{h^{-1}}$	Obeyesekere et al. (1999)	CPI degradation rate constant
19	a'_d	$0.41\ \mathrm{h^{-1}}$	Obeyesekere et al. (1999)	Cyclin D synthesis parameter (treated as a bifurcation parameter)

Table D2
Parameter values for the Bennett et al. model.

Index	Parameter	Value	Source	Description
20	K_R	25 μM	Bennett et al. (2005)	Effective dissociation constant for $P2Y_1$ receptor ATP binding
21	ν	0.12	Bennett et al. (2005)	background G-protein activation constant
22	K_G	8.82353	Bennett et al. (2005)	G-protein dissociation constant
23	r_h^*	2160 μM h^{-1}	Appendix D	IP_3 production rate
24	k_{deg}	225 h^{-1}	Appendix D	IP_3 degradation rate
25	V_{deg}	7200 μM h^{-1}	Gordon et al. (1986, 1989) and Joseph et al. (2004)	Michaelis constant (expected range 36–7200 μM h^{-1}, see Appendix D)
26	K_{deg}	50 μM	Gordon et al. (1986, 1989) and Joseph et al. (2004)	Michaelis constant
27	V_{ATP}	180,000 h^{-1}	Appendix D	ATP release rate constant
28	$[IP_3]_{min}$	0.013 μM	Bennett et al. (2005)	Minimum IP_3 concentration for ATP release
29	K_{rel}	10 μM	Bennett et al. (2005)	Kinetic parameter

Table D3
New parameter values for coupled model.

Index	Parameter	Value	Source	Description
30	γ	1 $\mu M^{-1} h^{-1}$	Appendix D	Calcium coupling strength (treated as a bifurcation parameter)
31	$[Ca^{2+}]_b$	0.0159835 μM	Fall et al. (2002)	Steady state calcium concentration
32	α	298.8 h^{-1}	Appendix D	ATP production rate constant
33	$[ATP_I]_{max}$	500 μM	Guthrie et al. (1999)	Maximum internal ATP concentration
34	ε	0.01 μM^{-1}		Stiffness of switch function
35	p_1	0.514987	Appendix A	Hill function coefficient
36	p_2	1.31319	Appendix A	Hill function coefficient
37	p_3	0.332195	Appendix A	Hill function coefficient
38	p_4	0.787902	Appendix A	Hill function coefficient
39	m	24.1946	Appendix A	Hill function coefficient
40	n	9.79183	Appendix A	Hill function coefficient
41	D_c	0.5	Appendix D	Critical Cyclin D concentration above which ATP is released (treated as a bifurcation parameter)
42	R_{sc}	1	Appendix D	Critical R_s concentration below which ATP is released (treated as a bifurcation parameter)

Appendix E. Initial conditions for Figs. 4, 5, 8, A2 and A3

	Fig. 4		Fig. 5		Fig. 8			
	(a, c)	(b, d)	(a, c)	(b, d)	Driving cell		Quiescent cell	
					(a, c)	(b, d)	(a, c)	(b, d)
$D(0)$	0.1205	0.1966	0.7720	0.7090	0.1197	0.3536	0.1023	0.1001
$E(0)$	2.1672	2.1958	0.3253	0.1949	0.0857	0.0392	2.1287	2.1541
$R(0)$	0.2787	0.2831	0.8574	0.8989	0.2721	0.8780	0.4686	0.4729
$R_s(0)$	0.9301	0.8928	1.2030	1.2119	0.9529	1.2656	0.9529	1.1758
$X(0)$	0.4608	0.4987	1.1141	2.8932	0.4033	0.4902	22.1852	0.4797
$[IP_3](0)$	0.013	0.9440	0.9440	0.0130	0.013	0.013	0.013	0.013
$[ATP_I](0)$	500	478.1865	478.1865	500	500	500	500	500
$[ATP_E](0)$	0	477.7613	477.7613	0	0	0	0	0

	Fig. A2		Fig. A3	
	(a, c)	(b, d)	(a, c)	(b, d)
$D(0)$	0.1554	0.7128	0.1602	0.5633
$E(0)$	1.2122	0.2218	1.0977	0.0672
$R(0)$	0.6277	0.8919	0.6501	0.9081
$R_s(0)$	1.1497	1.2088	1.1160	1.2394
$X(0)$	2.6821	2.3361	3.2614	12.1983
$[IP_3](0)$	0.013	0.013	0.013	0.013
$[ATP_I](0)$	500	500	500	500
$[ATP_E](0)$	0	0	0	0
$[Ca^{2+}](0)$	0.02	0.02	0.02	0.02
$h(0)$	0.9524	0.9524	1	1

References

Aktas, H., Cai, H., Cooper, G., 1997. Ras links growth factor signaling to the cell cycle machinery via regulation of Cyclin D1 and the Cdk inhibitor $p27^{Kip1}$. Mol. Cell. Biol. 17 (7), 3850–3857.

Baldin, V., Lukas, J., Marcote, M., Pagano, M., Draetta, G., 1993. Cyclin D1 is a nuclear protein required for cell cycle progression in G1. Genes Dev. 7 (5), 812–821.

Bennett, M., Farnell, L., Gibson, W., 2005. A quantitative model of purinergic junctional transmission of calcium waves in astrocyte networks. Biophys. J. 89 (4), 2235–2250.

Bittman, K., LoTurco, J., 1999. Differential regulation of connexin 26 and 43 in murine neocortical precursors. Cereb. Cortex 9 (2), 188–195.

BioModels database, http://www.ebi.ac.uk/biomodels-main/.

Boynton, A.L., Whitfield, J.F., Isaacs, R.J., 1976. The different roles of serum and calcium in the control of proliferation of BALB/c 3T3 mouse cells. In Vitro 12 (2), 120–123.

Chauhan, A., Legewie, S., Westermark, P.O., Lorenzen, S., Herzel, H., 2008. A mesoscale model of G1/S phase transition in liver regeneration. J. Theor. Biol. 252 (3), 465–473.

Chauhan, A., Lorenzen, S., Herzel, H., Bernard, S., 2011. Regulation of mammalian cell cycle progression in the regenerating liver. J. Theor. Biol. 283 (1), 103–112.

Chen, Z., Duan, R., Zhu, Y., Folkesson, R., Albanese, C., Winblad, B., Zhu, J., 2005. Increased Cyclin E expression may obviate the role of Cyclin D1 during brain development in Cyclin D1 knockout mice. J. Neurochem. 92 (5), 1281–1284.

Cheng, M., Olivier, P., Diehl, J.A., Fero, M., Roussel, M.F., Roberts, J.M., Sherr, C.J., 1999. The $p21^{Cip1}$ and $p27^{Kip1}$ CDK 'inhibitors' are essential activators of cyclin D-dependent kinases in murine fibroblasts. EMBO J. 18 (6), 1571–1583.

Csikász-Nagy, A., 2009. Computational systems biology of the cell cycle. Brief Bioinform. 10 (4), 424–434.

Dolmetsch, R.E., Xu, K., Lewis, R.S., 1998. Calcium oscillations increase the efficiency and specificity of gene expression. Nature 392 (6679), 933–936.

Dupont, G., 1998. Link between fertilization-induced Ca^{2+} oscillations and relief from metaphase II arrest in mammalian eggs: a model based on calmodulin-dependent kinase II activation. Biophys. Chem. 72 (1–2), 153–167.

Fall, C.P., Marland, E.S., Wagner, J.M., Tyson, J.J., 2002. Computational Cell Biology. Springer

Fam, S.R., Gallagher, C.J., Kalia, L.V., Salter, M.W., 2003. Differential frequency dependence of $P2Y_1$ and $P2Y_2$-mediated Ca^{2+} signaling in astrocytes. J. Neurosci. 23 (11), 4437–4444.

Gordon, E., Pearson, J., Dickinson, E., Moreau, D., Slakey, L., 1989. The hydrolysis of extracellular adenine nucleotides by arterial smooth muscle cells. Regulation of adenosine production at the cell surface. J. Biol. Chem. 264 (32), 18986–18995.

Gordon, E., Pearson, J., Slakey, L., 1986. The hydrolysis of extracellular adenine nucleotides by cultured endothelial cells from pig aorta. Feed-forward inhibition of adenosine production at the cell surface. J. Biol. Chem. 261 (33), 15496–15507.

Goto, T., Takahashi, T., Miyama, S., Nowakowski, R., Bhide, P., Caviness, V., 2002. Developmental regulation of the effects of fibroblast growth factor-2 and 1-octanol on neuronogenesis: implications for a hypothesis relating to mitogen–antimitogen opposition. J. Neurosci. Res. 69 (6), 714–722.

Gotz, M., Barde, Y., 2005. Radial glial cells defined and major intermediates between embryonic stem cells and CNS neurons. Neuron 46 (3), 369–372.

Gérard, C., Goldbeter, A., 2009. Temporal self-organization of the cyclin/Cdk network driving the mammalian cell cycle. Proc. Natl. Acad. Sci. U. S. A. 106 (51), 21643–21648.

Gérard, C., Goldbeter, A., 2011. A skeleton model for the network of cyclin-dependent kinases driving the mammalian cell cycle. Interface Focus 1 (1), 24–35.

Greenblatt, R., 2005. Human papillomaviruses: diseases, diagnosis, and a possible vaccine. Clin. Microbiol. Newslett. 27 (18), 139–145.

Guthrie, P., Knappenberger, J., Segal, M., Bennett, M., Charles, A., Kater, S., 1999. ATP released from astrocytes mediates glial calcium waves. J. Neurosci. 19 (2), 520–528.

Hazelton, B., Mitchell, B., Tupper, J., 1979. Calcium, magnesium, and growth control in the WI-38 human fibroblast cell. J. Cell Biol. 83 (2), 487–498.

Hung, J., Colicos, M.A., 2008. Astrocytic Ca^{2+} waves guide CNS growth cones to remote regions of neuronal activity. PloS ONE 3 (11), e3692.

Joseph, S., Pifer, M., Przybylski, R., Dubyak, G., 2004. Methylene ATP analogs as modulators of extracellular ATP metabolism and accumulation. Br. J. Pharmacol. 142 (6), 1002–1014.

Kahl, C., Means, A., 2003. Regulation of cell cycle progression by calcium/calmodulin-dependent pathways. Endocr. Rev. 24 (6), 719–736.

Kahl, C., Means, A., 2004. Regulation of Cyclin D1/Cdk 4 complexes by calcium/calmodulin-dependent protein kinase I. J. Biol. Chem. 279 (15), 15411–15419.

Kornack, D.R., Rakic, P., 1998. Changes in cell-cycle kinetics during the development and evolution of primate neocortex. Proc. Natl. Acad. Sci. U. S. A. 95 (3), 1242–1246.

Lagarias, J., Reeds, J., Wright, M., Wright, P., 1999. Convergence properties of the Nelder–Mead simplex method in low dimensions. SIAM J. Optim. 9 (1), 112–147.

Lanker, S., Valdivieso, M.H., Wittenberg, C., 1996. Rapid degradation of the G1 cyclin Cln2 induced by CDK-dependent phosphorylation. Science 271 (5255), 1597–1601.

Lee Rodgers, J., Nicewander, W.A., 1988. Thirteen ways to look at the correlation coefficient. Am. Stat. 42 (1), 59–66.

Li, H., Liu, T., Lazrak, A., Peracchia, C., Goldberg, G., Lampe, P., Johnson, R., 1996. Properties and regulation of gap junctional hemichannels in the plasma membranes of cultured cells. J. Cell Biol. 134 (4), 1019–1030.

Li, Y., Rinzel, J., 1994. Equations for $InsP_3$ receptor-mediated $[Ca^{2+}]_i$ oscillations derived from a detailed kinetic model: a Hodgkin–Huxley like formalism. J. Theor. Biol. 166 (4), 461–473.

Marpegan, L., Swanstrom, A., Chung, K., Simon, T., Haydon, P., Khan, S., Liu, A., Herzog, E., Beaulé, C., 2011. Circadian regulation of ATP release in astrocytes. J. Neurosci. 31 (23), 8342–8350.

Marquardt, D., 1963. An algorithm for least-squares estimation of nonlinear parameters. SIAM J. Appl. Math. 11 (2), 431–441.

Mishra, S., Braun, N., Shukla, V., Füllgrabe, M., Schomerus, C., Korf, H., Gachet, C., Ikehara, Y., Sévigny, J., Robson, S.C., et al., 2006. Extracellular nucleotide signaling in adult neural stem cells: synergism with growth factor-mediated cellular proliferation. Development 133 (4), 675–684.

Morris, T., DeLorenzo, R., Tombes, R., 1998. CaMKII inhibition reduces Cyclin D1 levels and enhances the association of $p27^{Kip1}$ with Cdk2 to cause G1 arrest in NIH 3T3 cells. Exp. Cell Res. 240 (2), 218–227.

Murray, A.W., Hunt, T., 1993. The Cell Cycle: An Introduction. Oxford University Press, New York

Nigg, E., 1995. Cyclin-dependent protein kinases: key regulators of the eukaryotic cell cycle. Bioessays 17 (6), 471–480.

Noctor, S., Flint, A., Weissman, T., Dammerman, R., Kriegstein, A., 2001. Neurons derived from radial glial cells establish radial units in neocortex. Nature 409 (6821), 714–720.

Novak, B., Tyson, J., 2004. A model for restriction point control of the mammalian cell cycle. J. Theor. Biol. 230 (4), 563–579.

Obeyesekere, M., Zimmerman, S., Tecarro, E., Auchmuty, G., 1999. A model of cell cycle behavior dominated by kinetics of a pathway stimulated by growth factors. Bull. Math. Biol. 61 (5), 917–934.

Patel, R., Holt, M., Philipova, R., Moss, S., Schulman, H., Hidaka, H., Whitaker, M., 1999. Calcium/calmodulin-dependent phosphorylation and activation of human Cdc25-C at the G2/M phase transition in HeLa cells. J. Biol. Chem. 274 (12), 7958–7968.

Patten, B.A., Peyrin, J.M., Weinmaster, G., Corfas, G., 2003. Sequential signaling through Notch1 and erbB receptors mediates radial glia differentiation. J. Neurosci. 23 (14), 6132–6140.

Pfeuty, B., 2012. Strategic cell-cycle regulatory features that provide mammalian cells with tunable G1 length and reversible G1 arrest. PLoS ONE 7 (4), e35291.

Rasmussen, C.D., Means, A.R., 1987. Calmodulin is involved in regulation of cell proliferation. EMBO J. 6 (13), 3961–3968.

Rasmussen, C.D., Means, A.R., 1989. Calmodulin is required for cell-cycle progression during G1 and mitosis. EMBO J. 8 (1), 73–82.

Rasmussen, G., Rasmussen, C., 1995. Calmodulin-dependent protein kinase II is required for G1/S progression in HeLa cells. Biochem. Cell Biol. 73 (3–4), 201–207.

Reigada, D., Lu, W., Zhang, X., Friedman, C., Pendrak, K., McGlinn, A., Stone, R., Laties, A., Mitchell, C., 2005. Degradation of extracellular ATP by the retinal pigment epithelium. Am. J. Physiol., Cell Physiol. 289 (3), 617–624.

Sheaff, R.J., Groudine, M., Gordon, M., Roberts, J.M., Clurman, B.E., 1997. Cyclin E-CDK2 is a regulator of $p27^{kip1}$. Genes Dev. 11 (11), 1464–1478.

Sherr, C., 1994. Gl phase progression: cycling on cue. Cell 79 (4), 551–555.

Sinal, S., Woods, C., 2005. Human papillomavirus infections of the genital and respiratory tracts in young children. Semin. Pediatr. Infect. Dis. 16 (4), 306–316.

Stacey, D., 2003. Cyclin D1 serves as a cell cycle regulatory switch in actively proliferating cells. Curr. Opin. Cell Biol. 15 (2), 158–163.

Stamatakis, M., Mantzaris, N., 2006. Modeling of ATP-mediated signal transduction and wave propagation in astrocytic cellular networks. J. Theor. Biol. 241 (3), 649–668.

Suprynowicz, F.A., Prusmack, C., Whalley, T., 1994. Ca^{2+} triggers premature inactivation of the cdc2 protein kinase in permeabilized sea urchin embryos. Proc. Natl. Acad. Sci. U. S. A. 91 (13), 6176–6180.

Swanson, C.A., Arkin, A.P., Ross, J., 1997. An endogenous calcium oscillator may control early embryonic division. Proc. Natl. Acad. Sci. U. S. A. 94 (4), 1194–1199.

Swat, M., Kel, A., Herzel, H., 2004. Bifurcation analysis of the regulatory modules of the mammalian G1/S transition. Bioinformatics 20 (10), 1506–1511.

Takahashi, T., Nowakowski, R.S., Caviness, V.S., 1995. The cell cycle of the pseudostratified ventricular epithelium of the embryonic murine cerebral wall. J. Neurosci. 15 (9), 6046–6057.

Thul, R., Bellamy, T.C., Roderick, H.L., Bootman, M.D., Coombes, S., 2008. Calcium oscillations. In: Cellular Oscillatory Mechanisms. Springer, pp. 1–27.

Tombes, R.M., Grant, S., Westin, E.H., Krystal, G., 1995. G1 cell cycle arrest and apoptosis are induced in NIH 3T3 cells by KN-93, an inhibitor of CaMK-II (the multifunctional Ca^{2+}/CaM kinase). Cell Growth Differ. 6 (9), 1063–1070.

Veylder, L., Joubès, J., Inzé, D., 2003. Plant cell cycle transitions. Curr. Opin. Plant Biol. 6 (6), 536–543.

Wang, J., Huang, X., Huang, W., 2007. A quantitative kinetic model for ATP-induced intracellular Ca^{2+} oscillations. J. Theor. Biol. 245 (3), 510–519.

Weissman, T., Riquelme, P., Ivic, L., Flint, A., Kriegstein, A., 2004. Calcium waves propagate through radial glial cells and modulate proliferation in the developing neocortex. Neuron 43 (5), 647–661.

Whitfield, J.F., Boynton, A.L., MacManus, J.P., Sikorska, M., Tsang, B.K., 1979. The regulation of cell proliferation by calcium and cyclic AMP. Mol. Cell. Biochem. 27 (3), 155–179.

Womac, A., Burkeen, J., Neuendorff, N., Earnest, D., Zoran, M., 2009. Circadian rhythms of extracellular ATP accumulation in suprachiasmatic nucleus cells and cultured astrocytes. Eur. J. Neurosci. 30 (5), 869–876.

Yang, K., Masahiro, Hitomi, Stacey, Dennis W., 2006. Variations in Cyclin D1 levels during the cell cycle determine the proliferative fate of a cell. Cell Div. 1, 32.